공학박사학위논문

Optimal Design of Sustainable Fischer-Tropsch Process Utilizing Micro-channel Technology

마이크로채널 기술을 이용한 지속가능한 피셔트롭쉬 공정 최적설계

2017년 2월

서울대학교 대학원

화학생물공학부

정 익 환

Abstract

Optimal Design of Sustainable Fischer-Tropsch Process Utilizing Micro-channel Technology

Ikhwan Jung

School of Chemical & Biological Engineering

The Graduate School of Seoul National University

Gas-to-liquid (GTL) has been considered a technology that converts natural gas into high value-added liquid fuel for decades. The produced fuel has less greenhouse gas emissions than the conventional gasoline or diesel after combustion, and the sulfur content is less than 0.5ppm. Therefore, it can be used as a clean fuel and environmentally friendly energy resource.

GTL process can be divided into a reforming process for producing synthesis gas, which is a mixture of carbon monoxide and hydrogen, from natural gas, and a Fischer-Tropsch (FTS) process for synthesizing a hydrocarbon chain. The key process is the Fischer-Tropsch synthesis, which requires a structure to deliver an effective heat removal because of the highly exothermic reaction (ΔH = -165 kJ /

mol). Generally, large scale commercial GTL processes are operated using a circulating fluidized bed reactor, a fluidized bed reactor, a multi-tubular fixed bed reactor, and a slurry column bed reactor.

In recent years, research on the reactor development with microchannel technology has been highlighted because it has been pointed out that existing reactors are hard to be applied to marine conditions in the development of offshore plant and microchannel reactors take advantages of high economical efficiency for small and medium scale processes.

Microchannel reactors can reduce the volume of existing reactors by a factor of 10 to 1000 times caused from reducing heat and mass transfer distances, increase the efficiency of the chemicals used in the process, make them environmentally friendly, easily control operation. By reducing the size of the reactor, space utilization can be widened through integration in the process, and productivity and process efficiency can be increased through modularization.

In this thesis, optimal design of reactor with microchannel technology and economical structure of Fischer - Tropsch stand-alone process are obtained. The optimal design of the cooling layer distributor that is the key of the heat removal performance is derived. The optimal reactor design that can satisfy both the reaction safety and the miniaturization of the reactor core part is proposed. From the viewpoint of process, superstructure process modeling with microchannel reactor was carried out and optimization process was conducted to find the most economical process. The reactor model was validated using real reactor operation

data.

First, a simple trapezoidal-shaped guiding fin was optimized and applied to the manifold to ensure a uniform coolant flow to the cooling layer inside the stacked microchannel reactor. It was possible to achieve a stable distribution even over a large area of over 100 channels by using the principle of inducing mixing by appropriately transferring the refrigerant fluid introduced into the guiding fin to a space defined as a free mixing zone. Specifically, we performed optimization using the artificial neural network as a surrogate model for the structure of the guiding fin. Furthermore, we conducted a robustness test on the flow rate, fluid type, and operating temperature for the optimal structure. As a result, $500 \leq \mathrm{Re}_{GF} \leq 10800$ Uniformity of the distribution could be maintained in a considerably large area.

Next, the reactor core was modeled by introducing a cell-coupling method, and multi-objective optimization was performed on seven design variables with the maximum reaction temperature rise and reactor core volume as an objective function. The maximum reaction temperature rise is related to keeping isothermal condition (anti-hotspot) of the reactor and the reactor core volume is directly related to reactor compactness. As a result of the optimization, the Pareto optimal points can be obtained. As the maximum temperature rise increases, the reactor length becomes short and the width increases, and the height is generally constant. These optimization procedure can be used to determine two factors. First, the reasonable coolant flowrate can be obtained from the comparison among the optimal Pareto point set with the sensitivity analysis. Furthermore, it was possible

to prioritize the design factors related with reactor durability.

Finally, a superstructure FTS stand-alone process model with various processes such as single or multistage FTS, recycle and water gas shift reaction, which has been studied extensively in order to improve the process efficiency, is optimized to maximize the profitability. The optimal design was obtained by introducing Genetic Algorithm. As a result of further sensitivity analysis based on changes in raw material costs and product prices by deriving additional two representative systems (multi-stage and single-stage without recycle process), a single stage with recycle is absolutely superior in all cases.

This study has a great contribution to the design and operation of an exothermic reactor using microchannel technology and a Fischer - Tropsch process.

The both of optimal design procedures of the cooling layer with high robustness on uniform distribution and the reactor miniaturization with stable operation deliver great value in designing and operating the optimal microchannel reactor design. In addition, the proposed design procedure for economical Fischer Tropsch system can be used as a process design package with the reactor design methodology.

Keywords: micro-channel reactor, distributor modeling, uniform distribution, Fischer-Tropsch reactor modeling, reactor optimization, Fischer-Tropsch synthesis process, superstructure process optimization

Student ID: 2014-31095

Contents

List of Figures

List of Tables

CHAPTER 1: Introduction

1.1. Research motivation

Gas to liquid(GTL) process has been attracting much attention in recent decades as a technology to convert natural gas into environmentally friendly, high value-added liquid fuel. The most important process in the GTL process is the Fischer-Tropsch synthesis (FTS) process, which requires an effective heat removal design at the reactor level because of the highly exothermic reaction (ΔH = -165 kJ / mol). In recent years, researchers have been studying microchannel-based reactors, which are superior in terms of volume to heat transfer area for applications in marine and small- to medium sized plants. The microchannel FTS reactor is a system in which a process layer and a cooling layer are alternately stacked. The process layer is packed with a catalyst and the FT reaction occurs on the catalyst surface due to the introduction of syngas. The heat generated is absorbed to the abutting cooling layers. These technology is mainly led by Velocys Inc. and CompactGTL in reactor structure and reaction catalyst field.

In order to achieve the sustainable FTS process, the most important thing is to satisfy stable reactor operation and highly profitability. That is, it is necessary to design a stable operation from the reactor point of view and to construct a process with high profitability using these reactors.

For the stable operation of reactor, the isothermal condition of the reactor must be

ensured. The following two conditions must be satisfied.

1) Flow uniform distribution & robustness

2) Effective reaction heat removal design

First, to satisfy the condition 1), it is necessary to design an intuitive, simple but high-performance distributor. In the header section, the primary distributor, a commercially developed T-shaped distributor is often used in the industrial field and it can be applied. However, there is no manifold design study for the layer inside manifold design, especially for large microchannel reactor layers with more than 100 channels. The manifold needs to be robust against various fluid flow conditions and it is necessary to derive a simple structure of manifold design that combines ease of fabrication.

Next, to maintain the reaction stability from the viewpoint of the whole reactor, an effective design which can lower the maximum rise of the reaction temperature is required for satisfaction of the condition 2). The design of the existing microchannel Fischer-Trospch (FT) reactor first determines the basic design factors such as channel height, width and length in the single channel analysis stage, and the complex heat transfer and momentum analysis between cooling and reaction channels in multi-channel analysis. The design factors are analyzed separately and sequentially. The optimal design derived in the early stage of the design and those factors cannot still guarantee the optimum in multi-channel analysis stage. Besides, the analysis in multi-channel stage more than 1000 channels has the limitation of thousands of cases since thermal effect analysis is conducted using computational

fluid dynamics. In many cases, comparing designs to design leads to limitations in effective decision-making. Therefore, it is necessary to determine the optimal design range considering high operating safety and reactor efficiency in a short time.

Lastly, many FTS process studies have been generally conducted to increase carbon efficiency because it is aimed to produce hydrocarbon fuel by utilizing carbon source. In order to obtain sustainability, it is necessary to derive a process with high profitability in these various studies.

Therefore, we tried to solve the above three issues by using various optimization techniques in this study.

1.2. **Research objectives**

The objective of this thesis is to derive an optimal design of sustainable FTS stand-alone system using a microchannel FT reactor. In the layered manifold design of the reactor, a guiding fin of simple shape is applied to both the inlet and outlet of the cooling layer, and a structure capable of achieving uniform flow over a large area distribution over 100 channels is proposed and analyzed by computational fluid dynamics. A robustness test is carried out on the proposed optimal distributor design for flow, fluid type, and operating temperature. In order to maintain the stable operation on the reactor, an effective design that can lower the maximum process temperature rise is required, and the miniaturization of the

reactor must be considered for the advantage of the characteristics of the microchannel reactor. Seven design variables that can represent the entire structure of the reactor are determined, and optimization is performed to minimize the reactor core volume (compactness) and the maximum temperature rise of the reaction channel (safety) simultaneously. In the optimization of FTS stand-alone process, the superstructure process which can consider single stage, multi stage FTS, recycle, and water gas shift reaction is constructed and economically most advantageous FTS structure by using Genetic Algorithm is obtained

1.3. **Outline of the thesis**

The thesis is organized in sequence of optimal design procedure from microchannel reactor to entire process system. The details are as follows. Chapter 1 provides research motivation and objective. In chapter 2, the optimal design of cooling layer for uniform flow in microchannel FT reactor is described. The simple trapezoidal-shaped guiding fin is applied in manifold area and optimized using artificial neural network as surrogate model. Chapter 3 presents that the reactor core was modeled by introducing a cell-coupling method, and multi-objective optimization was performed on seven design variables with the maximum reaction temperature rise and reactor core volume as an objective function. Chapter 4 describes that a superstructure FTS stand-alone process model integrated with various key processes proposed in previous studies is optimized to maximize the

profitability. Chapter 5 presents the conclusion and an outline for the future works.

CHAPTER 2: Optimal design of cooling layer in microchannel Fischer Trospch reactor

2.1. Background

Offshore gas to liquid (GTL) process for the development of associated and stranded gas reservoir has been recently spotlighted[1-3]. It is mainly focused to make the reactor more compact with introduction of microchannel-type equipment especially on Fischer-Trospch(FT) reactor that is required to remove the heat from highly exothermic reaction as following.

$$CO + H_2 \rightarrow -CH_2 - + H_2O \qquad \Delta H_{CO\,reacted} = -165\ \mathrm{kJ/mol} \qquad (2-1)$$

Microchannel type reactor shows more effective on heat and mass transfer performance resulted from shortening the distance between neighboring heat sink and source channels than typical reactors such as slurry bubble column bed, multi-tubular fixed bed, fluidized bed reactor. Its technology can bring around 10-1000 times reduction of reactor volume based on typical reactor, the intensification of space utilization caused from effective process arrangement as well as the improvement of productivity and performance[4-6].

It is critical to keep the reactor isothermal condition by effective heat removal since microchannel FT reactor is staked of cooling and process layers in alternate fashion, which results to highly complicated interaction in terms of heat and mass transfer between neighboring channels and layers[7-12]. Some analyses focused on

heat and mass transfer among neighboring channels or on entire reactor typically are conducted under the assumption of ideal uniform distribution of fluid within channels[10-12]. In reality, on the other hand, it is difficult evenly to remove the heat revealed from adjacent process layers with possibility of maldistribution. It might cause the hotspots and runaway reaction brought from inequality of the heat removal capability each coolant channel has, which leads to poor performance and selectivity. It is essential to design the coolant distributor layer inducing uniform distribution under wide robustness of operating condition[13].

In the literature researching fluid uniform distribution in microchannel type equipment, the majority is mainly focused on the development of manifold design for uniform distribution. Tonomura. et al. conducted CFD parametric study of the manifold shape in Z-type microchannel device with 5 channels and optimization with minimization of manifold area constrained uniform distribution[14]. Cheng et al. reported CFD-based optimal manifold design by simplified conjugate gradient method with 44 discretized geometrical variables for triangle-shaped manifold in micro-reformer having 68 channels[15]. Zhang et al. suggested modified manifold by applying additional cavity on inlet part of conventional guiding channel of plate fin heat exchanger with 30 channels. Experiments are conducted to get the improved uniformity on various ratio of cavity to distributor height[16]. Pan et al. carried out the sensitivity analysis on the geometric variables of rectangular-shaped manifold and main channels in micro-device with 10 channels to deduce the uniformity condition[17]. They proposed that the right triangle manifold was the most effective

on flow uniformity among various types of triangular type manifold in micro-device with 20 channels[18]. There is, however, almost no study dealing with distributor design and robustness analysis for the large scale of microchannel type layer with over 100 channels. It is guaranteed for distributor to be simple and effective design for flow uniformity since the critical requirements of the practical scale-up for commercial scale are simplicity and robustness for wide variation of operating condition.

In this chapter, trapezoid-shaped simple guiding fin is proposed to achieve flow uniformity in the manifold of U-type microchannel layer having 110 channels. The geometrical effect of free mixing zone directly fixed by the shape of guiding fin is analyzed using ANSYS® CFX 15.0, commercial CFD program. In detail, turbulent mixing is formed within free mixing zone to change the inlet flow momentum into 110 main channels. Optimization of simple guiding fin is conducted using artificial neural network (ANN) and compared with previous literature. Lastly for the robustness for wide industrial use is tested with respect to change of flowrate, flow property.

2.2. **Model description**

Basic microchannel FT reactor is constructed with 30 stacked cells each of which consists single process and cooling layer as shown in Figure 2-1a. Its orientation is paralleled with gravity because hydrocarbon product converted from synthesis

gas(syngas) inflowing downward from upper side of reactor is dropped by gravity.

Fin shaping main channels is inserted inside both process and coolant layer in order to enhance heat transfer from process layer to coolant layer.

In this study, the scope of interest is manifold geometry with introduced simple guiding fin in U-type coolant layer in Figure 2-1b. It is valid with following 2 conditions assumed.

- ✓ Well-designed coolant header is used for uniform distribution from the pipe into each coolant layer.
- ✓ Coolant flowrate is large enough effectively to remove revealed heat from process layer within 1 ℃ as temperature difference between coolant inlet and outlet for nearly isothermal reactor condition.

First assumption is easily achievable with enough large coolant pipe as well as reactor assembly of evenly fabricated cell layers. In case of the second assumption, 200 LPM of Syltherm 800 which is highly stable thermal fluid for sustainable operation is pumped into coolant pipe in operating condition specified in Table 2-1. The low temperature FT reaction occurs in process layer and target productivity of C_{5+} is around 0.2 BPD. Baseline flowrate of 200 LPM provides negligible temperature rise which can be considered under the condition of constant fluid property. It can lead to be focused only on fluid dynamics except heat transfer.

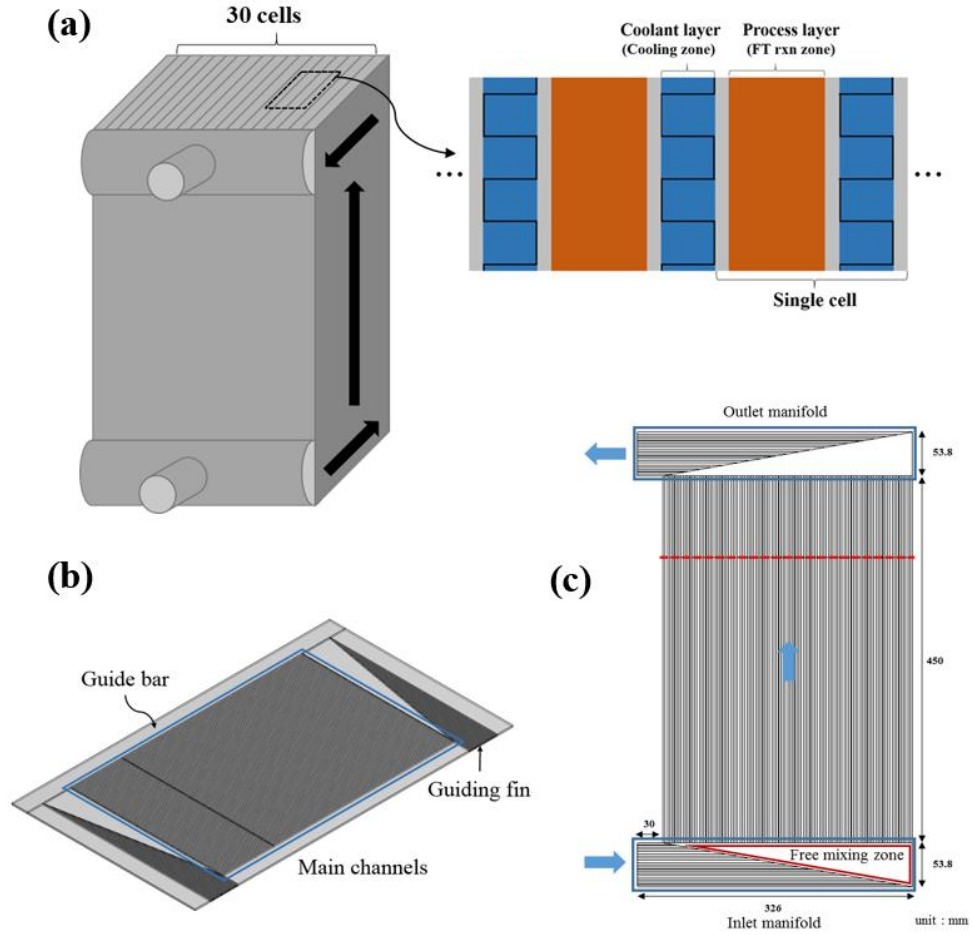

Figure 2-1.Microchannel Fischer-Tropsch reactor geometry: (a) Entire reactor core; (b) Coolant single layer; (c) Coolant fluid region

Figure 2-1c is the fluid region for CFD analysis. Governing equations are Navier-Stokes equation for momentum conservation (2) and continuity equation for mass conservation (3).

$$\rho\frac{\partial \mathbf{u}}{\partial t} + \rho\mathbf{u}\cdot\nabla\mathbf{u} = -\nabla p + \mu\nabla^2\mathbf{u} - \rho\mathbf{g} \quad (2-2)$$

$$\nabla\cdot\mathbf{u} = 0 \quad (2-3)$$

where ρ is coolant density [kg/m^3], $\mathbf{u}$ is fluid velocity vector [m/s], p is pressure [bar], μ is dynamic viscosity of coolant fluid [Pa s], $\mathbf{g}$ is gravitational acceleration [m^2/s]. The solver settings are no slip wall condition, no reaction, Shear stress transport turbulence model. ANSYS CFX® 15.0 is used as commercial CFD code and it is run on the computer specifying E5-2697V2 2.7 GHz CPU 12 Core / 256 GB DDR3 RAM.

Simple guiding fin introduced in the inlet and outlet manifold is generally chosen of the same shape, size, and material (SS316) with main channel for ease of fabrication. The dimension of coolant fluid region is specified on Figure 2-1c and Table 2-2. Total number of main channels that is formed by inserted fin is 110 and that of guiding channels is 20. The number of guiding fin channels was fixed for problem simplification. Generally, as the number of channels increases, the flow rate of coolant flowing through each channel is lower, so that the momentum change becomes less. It would be advantageous on distribution but disadvantageous on reactor compactness. It is better to be fixed with lower number. The guide bar for strong bond with both sides of process layers is placed along the

borders except inlet and outlet. At that position, bonding is made by guiding fin instead of guide bar.

Table 2-1. Baseline coolant property and operating condition

Fluid property (Syltherm 800)		**Operating condition**	
MW (g/mole)	271.2	Pressure (barg)	10
Density (kg/cum)	744.3	Inlet Temperature (℃)	230
Viscosity (Pa-s)	0.00081	Inlet flowrate (LPM)	200

Table 2-2. Dimensions of fluid region

Position		Value (mm)
Main channels	Length	450
	Height	3.05
	Single width	2.6
	Total width	326
	Thickness	0.1
Guiding channels	Single width	2.6
	Total width	53.8
Guide bar width		30

The upper (P) and bottom length (Q) of guiding fin are determined as the most effective geometric variables based on simplicity shown in Figure 2-2 because overall shape can be directly changed by them. The width of inlet, guide bar and dimension of main channels are fixed. Length P and Q are started from the each corner of inlet side and extended toward the opposite side of inlet. For the convenience of analysis, representative boundary positions are indicated and detailed location is specified in Table 2-3. The feasible range of P and Q is stated bellow.

$$0 \leq \mathrm{P(mm)} \leq 30 \qquad (2-4)$$

$$30 \leq \mathrm{Q(mm)} \leq 326 \qquad (2-5)$$

The reason why upper bound of P is boundary position C is that the part of main channel would be physically blocked if P is lengthened beyond the boundary point C. The lower bound of Q is set at the boundary position E since the guiding fin is useless and not effective on distribution. For additional operation convenience, the guiding fin geometry is symmetrically applied to both inlet and outlet manifold.

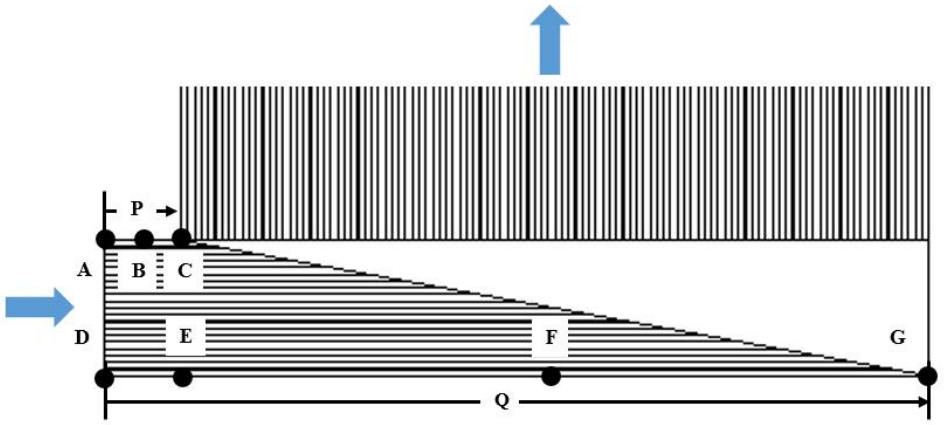

Figure 2-2. Geometric variables P, Q and boundary positions A, B, C, D, E, F, G in inlet manifold

Table 2-3. Boundary point information

Boundary position	**P (mm)**	**Q (mm)**	**Note**
A	0	-	Inlet corner position starting P and lower limit of P
B	15	-	Mid-point of A and C
C	30	-	Upper limit position of P
D	-	0	Inlet corner position starting Q
E	-	30	Lower limit of Q
F	-	178	Mid-point of E and G
G	-	326	Upper limit position of Q

The flowrate in each main channel is measured at the bold red dashed line indicated in Figure 2-1c where fully developed pipe flow sufficiently occurs. Distribution index, S is widely used for uniform performance estimator [15, 16, 18-20].

$$S = \sqrt{\frac{1}{N-1}\sum_{i=1}^{N}\left(\frac{\mathrm{F}_i}{F_{avg}} - 1\right)^2} \qquad (2-6)$$

$$F_{avg} = \frac{1}{N}\sum_{i=1}^{N} F_i \qquad (2-7)$$

where S is distribution index, F_i is flowrate of i-th channel, F_{avg} is average flowrate of entire main channels, N is the total number of main channels. It indicates close uniform flow as S approaches to 0 which is perfect uniform distribution.

The work flow of present study is shown in Figure 2-3. Firstly, it is conducted for geometric case study to see the effect of the existence and sensitivity of guiding fin size with varying P, Q in feasible range on the flow distribution in main channels. Next, the optimal design of guiding fin for uniform distribution is gained using Matlab optimization code and ANN fitting with CFD simulations. Lastly, the robustness test concerning the variance of flowrate, fluid property is performed to identify the feasible variation range of operating condition under the guarantee for uniform flow, which is one of the critical feature of distributor for industrial use.

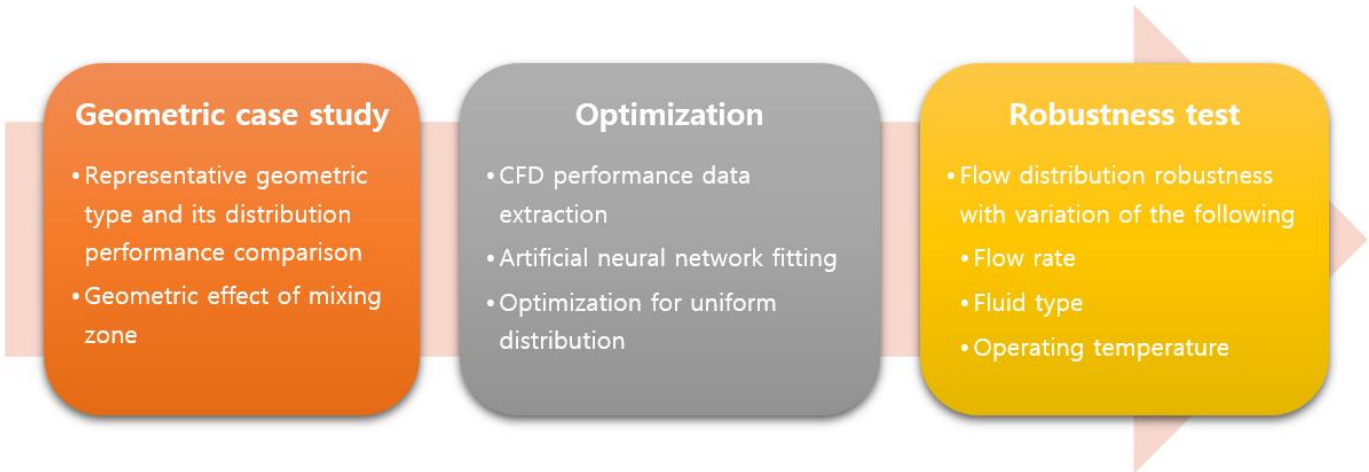

Figure 2-3. Study work flow

2.3. **Case study**

In this chapter, the effect of guiding fin geometry on flow distribution in main channels is investigated with varying P, Q.

2.3.1. Extreme cases

It is required to verify the clear influence of the guiding fin existence. Figure 2-4 indicates velocity contour on entire fluid domain of 2 extreme cases. (a) is for the case of no fin introduced (P = 0, Q = 0). The other case (b) is that the full fin(P = 30, Q = 326) is applied on both manifolds symmetrically. Both normalized flow distributions results are plotted in Figure 2-5. Type 1, Type 2 distribution are for no fin, full fin case respectively. Channel position of x-axis is indicative of labelling main channel that 1 is the nearest channel from fluid inlet and, 110 is furthermost one. In no fin case, the severe maldistribution occurs with leaning around 2.3 times toward channel position 1 in comparison to ideal average flowrate. It leads to uneven run-away reaction and hot spots in process layer directly related with low product yield, hazardous operation because relatively low flowrate has smaller heat transfer coefficient than high flow rate with overcooling. The flow pattern leans to main channels near inlet in U-type layer where relatively short flow path with low flow resistance is made. Whereas, the opposite but still severe maldistribution is shown in full fin one. The turbulent mixing ($Re_{FMZ} = 3646$) starts to occur in Free mixing zone (FMZ) shown in Figure 2-1c. The guiding fin plays a role of moving

the starting point of coolant inflow from inlet line (A-C) to extended line (P-Q) without mixed with other neighboring streams. That is, it is considered a flow transport device to resolve the inherent maldistribution the large scale microchannel manifold of no fin case has.

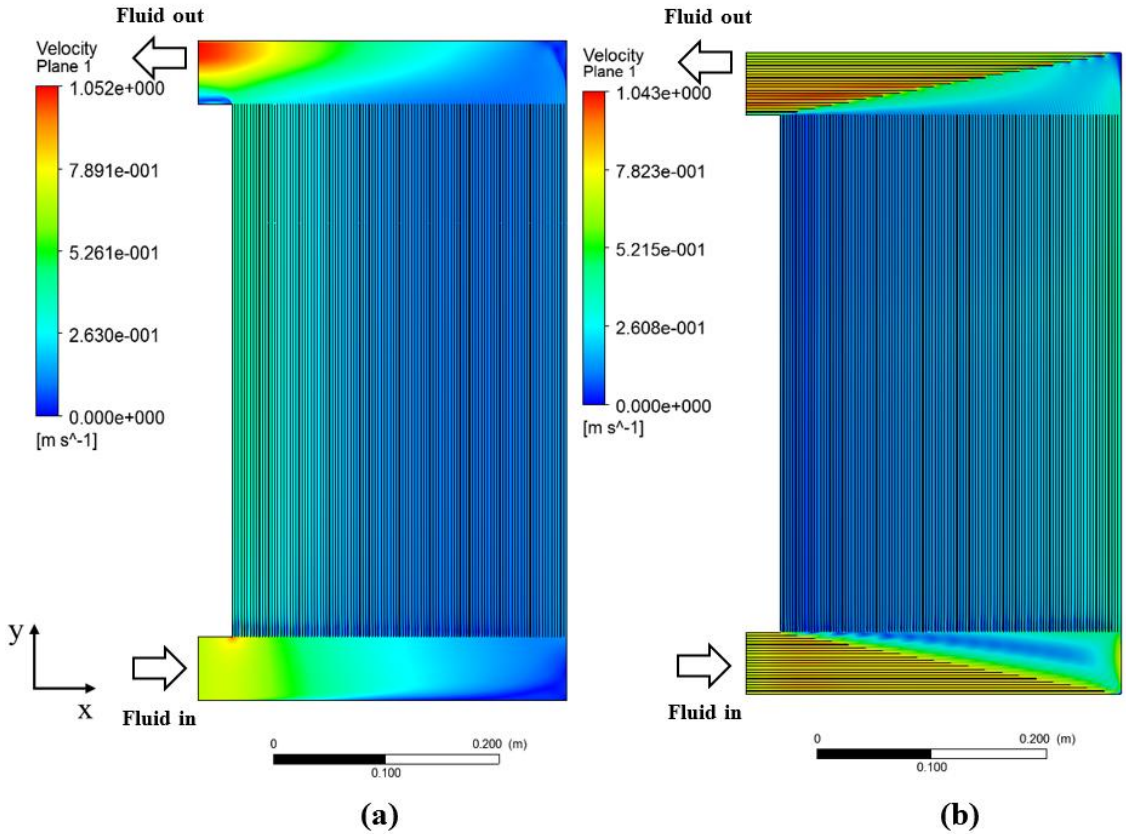

Figure 2-4. Extreme distribution cases: (a) No fin case; (b) Full fin case

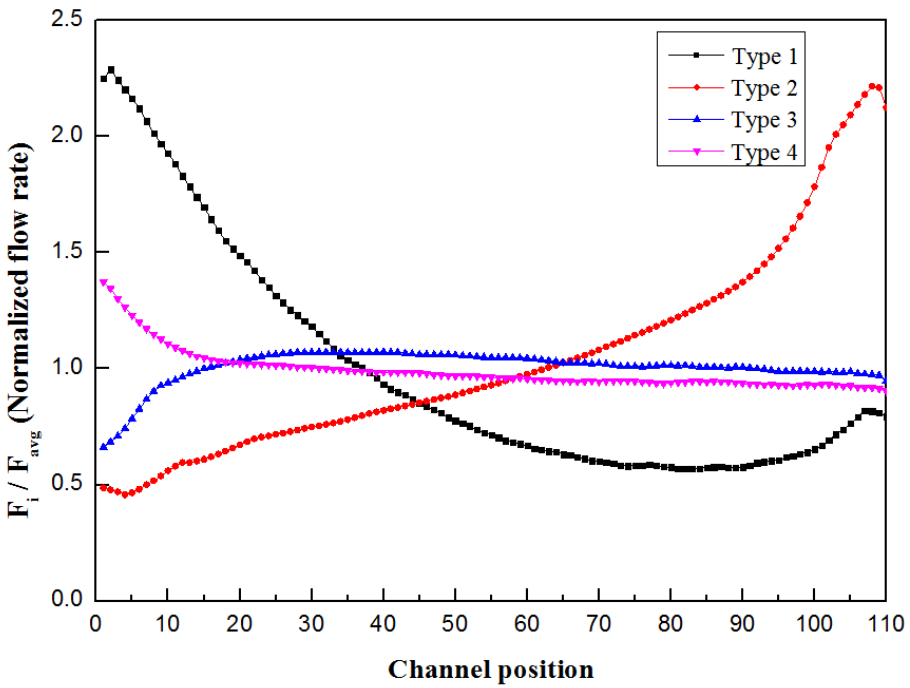

Figure 2-5. Representative types of flow distribution depending on design variables P, Q

2.3.2. Fin geometry variation

Figure 2-5 and Table 2-4 is types of representative distributions in case that P, Q are located at each boundary position. Both Type 1 and Type 2 shows the extreme cases of maldistribution mentioned above. In type 2 distribution, the flow leans toward near channel position 110. The inflow coming out of guiding fin is bumped against the wall and re-distributed into main channels. The energy cannot help being focused on the entrance of channel position 110.

With respect of momentum, the coolant inflow directly coming out of guiding fin has only x-direction inertia momentum without y-direction one. In FMZ, momentum change to y-direction occurs by the turbulent mixing. For the achievement of ideal uniform distribution, the fully momentum change required to arise when the all the flow passing through the entrance of main channels has fully y-direction momentum. As seen in Type 2 distribution, the reason why the inflow crushed into the wall near channel position 110 is that there is not enough space to change the momentum direction. On the other hand, the flow in Type 1 distribution leans to main channels near channel position 1 even though it has the largest FMZ. Before most inflow approaches to channel position 110, its momentum is fully changed with influence by U-type characteristics that the flow path near inlet is the shortest. The guiding fin is required to be introduced to transport some of inflow keeping no momentum change. Accordingly, sufficiently balanced space of free mixing zone is the most important factor to change the momentum direction since

the inflow direction(x-direction) and main channel direction (y-direction) are perpendicular.

In order to reduce the flow crushed on the wall in Type 2 distribution as well as to increase the flow reaching channel 110 in Type 1 distribution, Q is placed at boundary position F. It means that A-C-F-D shaped guiding fin is inserted, which makes Type 3 distribution. The distribution near the wall becomes almost flat. The amount of reduced flow compared to Type 2 distribution is evenly distributed for all over the main channels. In the view of momentum, sufficient space of FMZ is made to interrupt the crushed flow on the wall with complete momentum change almost right before reaching the wall. With comparison to Type 1, applied guiding fin with prolonged bottom length makes the coolant inflow be carried to the middle of manifold with maintaining the x-direction momentum inertia. After coming out from the guiding fin into the FMZ, coolant inflow is mixed with reduction of momentum inertia in x-direction and increase of y-direction one. It becomes known that Q directly influences the distribution near channel position 110 and slightly gives the effect on the rest of channel positions.

Table 2-4. Flow distribution types and corresponding geometry

Flow distribution type	**Guiding fin geometry (Boundary point connected figure)**	**P / Q**
Type 1	No fin (-)	0 / 0
Type 2	Full fin (A-C-G-D)	30 / 326
Type 3	Half fin 1 (A-C-F-D)	30 / 178
Type 4	Half fin 2 (A-F-D)	0 / 178

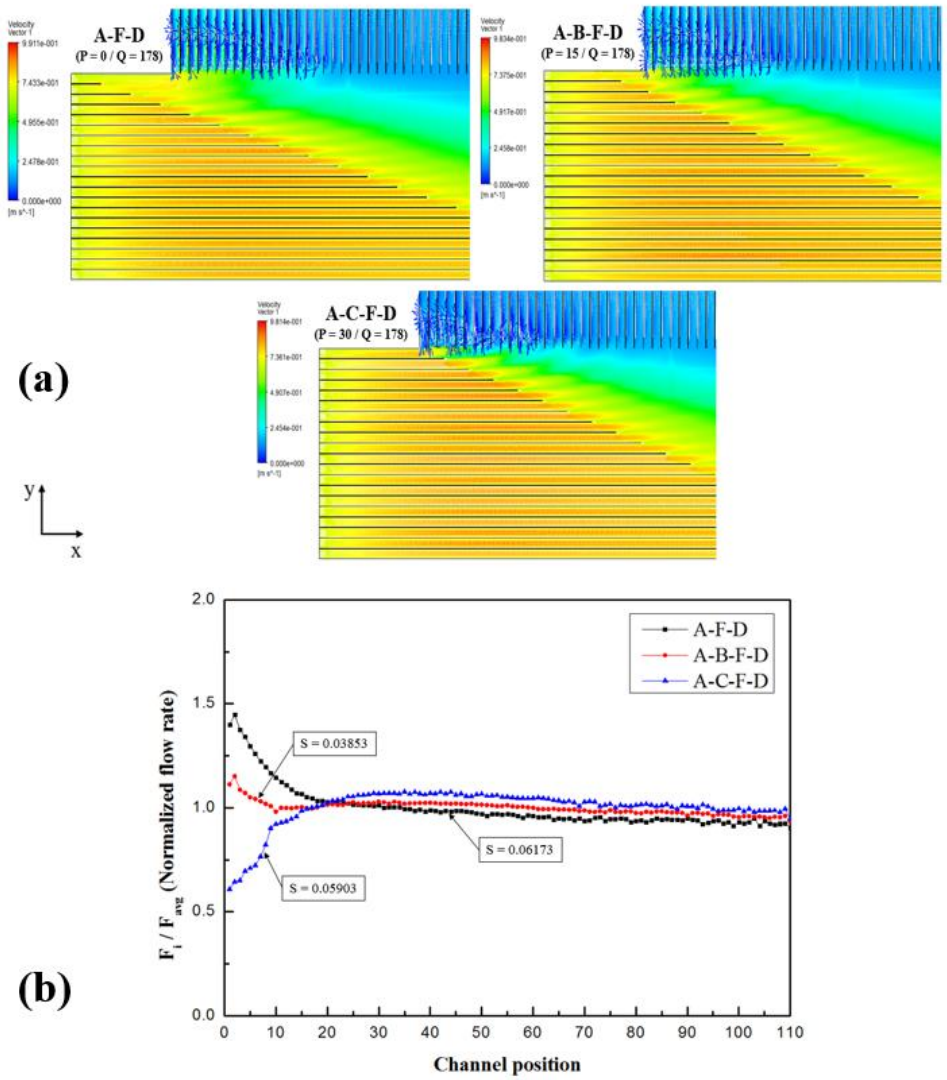

Figure 2-6. Fluid velocity vector diagram near inlet guiding fin (a) and flow distribution diagram (b) varying P with Q fixed at boundary point F

In the distribution near channel position 1, maldistribution is slightly improved by influence of balanced distribution near channel position 110, but still insufficient flow exists. As the same way with shortening Q to reduce crushed flow on the wall, length P decreases to 0 mm from Type 3. It means A-D-F (right triangle)-shaped guiding fin is introduced, which is Type 4 distribution. It rarely gives the distribution influence near channel position 110 since modified guiding fin can't physically affect the momentum change of bottom inflow and the length change difference with comparison to Q is 6 times smaller. Whereas, it seriously affects the distribution near channel position 1 despite small change. In the same phenomenon, increased flow near channel position 1 comes from the rest of main channel flow. Consequentially, geometric variable P and Q mainly affect the flow distribution near channel position 1 and 110 respectively.

For detailed view of flow near the channel position 1, the end point of P is placed at boundary position A, B, C with that of Q fixed at boundary position F as shown in Figure 2-6. Figure 2-6a is the velocity vector diagram for guiding channels, 33 main channels, and corner of FMZ. In A-F-D shaped guiding fin case, there are sufficient space to mix the coolant flows in the channels near upper inlet stream before reaching channel position 1. It provides increased flow into main channels near channel position 1 with momentum changed. Whereas, a little overflow occurs as seen in Figure 2-6b. It results to partial maldistribution near inlet. The extension of P would reduce the overflow with reduction of the space of FMZ. For extreme case, the ending point of P is located boundary position C. It

leads to no mixing space before channel position 1. The insufficient flow is induced due to low momentum change. Thus, P has to be properly located between boundary position A and C to adjust the flow distribution near channel position 1. In case that the ending point of P is on boundary point B(A-B-F-D shaped guiding fin), the nearly uniform distribution is achieved. It caused from the sufficient mixing space for momentum change on the balanced amount of flow.

There are backflows in the entrances of channel position 1 – 15 as seen in Figure 2-6a. This phenomenon occurs since the fast flow in upper stream of guiding fin is physically bumped into the entrance wall with insufficient space to change momentum. It leads to the unstable distribution near main channels for all the 3 cases indicated in Figure 2-6b. It is considered geometrically inherent distribution near the inlet.

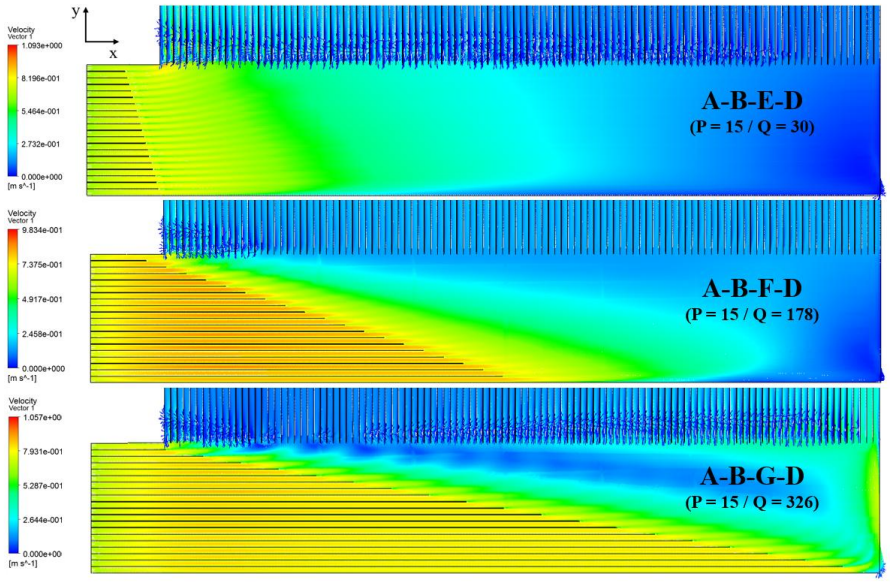
y
x
Velocity
Vector f
1.093e+000
8.196e-001
5.464e-001
2.732e-001
0.000e+000
[m s^-1]
A-B-E-D
(P = 15 / Q = 30)
9.834e-001
7.375e-001
4.917e-001
2.458e-001
0.000e+000
A-B-F-D
(P = 15 / Q = 178)
1.057e+00
7.931e-001
5.287e-001
2.644e-001
0.000e+00
A-B-G-D
(P = 15 / Q = 326)

(a)

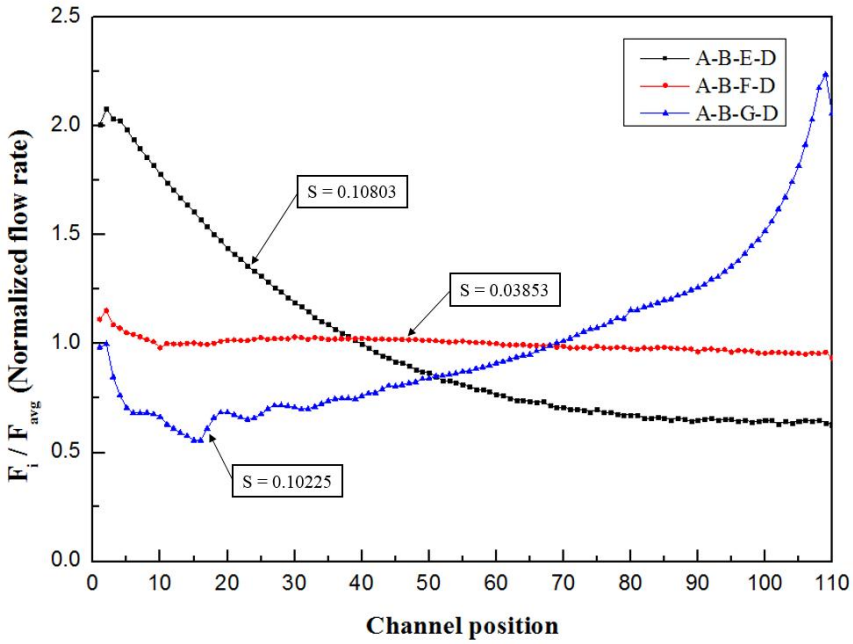
A-B-E-D
A-B-F-D
A-B-G-D
S = 0.10803
S = 0.03853
S = 0.10225
F_i / F_avg (Normalized flow rate)
Channel position
0.0
0.5
1.0
1.5
2.0
2.5
0
10
20
30
40
50
60
70
80
90
100
110

(b)

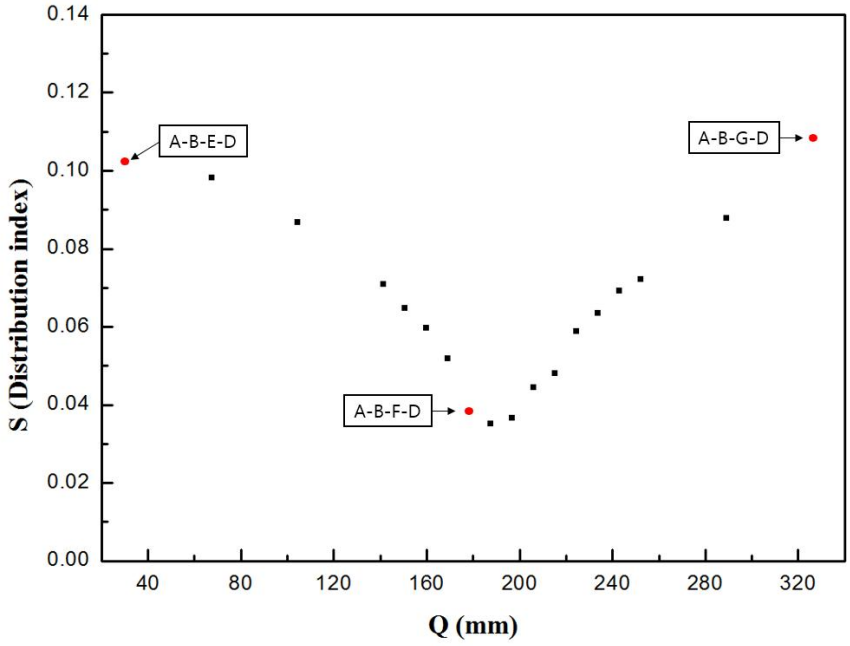

(c)

Figure 2-7. Fluid velocity vector diagram near inlet guiding fin (a), flow distribution plot (b) and distribution index plot (c) varying Q with P fixed at boundary point B

For detailed analysis of Q effect, the ending point of Q is varied on boundary position E, F, G with that of P fixed at boundary position B shown in Figure 2-7. It substantially affects the size of FMZ directly related with turbulent mixing for momentum change. In the case of A-B-E-D shaped guiding fin, the largest FMZ fully helps momentum change of most flow to occur before approaching to the wall opposite to inlet shown in Figure 2-7a and b. Its distribution is considered Type 1 distribution since that is almost same as the no fin case exception slightly reduced maldistribution near channel position 1. The rare flow exists in the corner at boundary point G. That means the short Q can't transport the flow to the region far away from the inlet. In the other case of A-B-G-D, its distribution is also similar with Type 2 distribution. Flow dash on the wall exists and leads to redistribute the flow into main channels in reverse x-direction. On the other hand, the distribution of A-B-F-D case shows the nearly uniform flow with the proper transportation length of Q.

In Figure 2-7a, the serious backflow generally occurs at the entrances of main channels of A-B-E-D and A-B-G-D guiding fin compared with A-B-F-D behind channel position 30. This phenomenon has different feature from the one near inlet and considered not to be inherent unstable distribution. It is caused from unbalanced flowrates among neighboring inlets of main channels. It can be explained using Bernoulli's equation (8).

$$\frac{\partial}{\partial s}\left(\frac{v^2}{2}+\frac{p}{\rho}+g\cdot h\right)=0 \qquad (2-8)$$

For region between inlet and outlet of 110 main channels, the potential energy is same. Then the sum of kinetics and pressure energy is equal to constant. The static pressures at the outlet of main channels are not significantly different. If the flowrate in any channel position is different from that in neighboring channels, the high pressure gradient is generated near inlets of main channels. The back flow can be seen only at the maldistribution region behind channel position 30 shown in Figure 2-7b.

Figure 2-7c presents the distribution index result of the various length of Q with the ending point of P fixed at boundary position B. Too small and large Q make severe maldistribution with over 0.1 of distribution index, whereas the flow uniformity gets increased with approaching to the close middle point of Q even below A-B-F-D guiding fin result. Thus, it is possible to get the close optimal design near the middle of Q.

2.4. **Optimization of guiding fin geometry**

There is an optimal design of guiding fin to achieve the uniform distribution with respect to geometric variables P, Q that can adjust local distribution on near and far from coolant inlet. The optimal problem can be defined as stated below.

$$\text{minimize} \quad S(P,Q) \qquad (2-9)$$

$$\text{s.t.} \quad 0 \leq P \leq 30 \qquad (2-4)$$

$$30 \leq Q \leq 326 \qquad (2-5)$$

Actually, S is extremely nonlinear function of flowrate, fluid property, geometric variables, channel geometry and number.

In this study, S is still nonlinear function affected by turbulence mixing and channel geometry leading to complex flow behavior even though the rest of variables are constant except for geometric variable P, Q. Each of simulation point has high calculation load with approximately 19 billion of mesh elements. 122 of pre-calculated simulation data can be used as representative points to build empirical model by regression. Artificial neural network (ANN) is employed because it is widely used for highly nonlinear function fitting. Target variable is S and inputs are P, Q. Figure 2-8 shows the schematic diagram and activation function of ANN applied on present study. For the fitting accuracy, the sufficient number of hidden layer is set as 10. Tan-sigmoid function (Eq. 2-10) which is widely used as nonlinear activation function is applied and regressed function is calculated by Eq. 11, 12.

$$F(u) = \frac{2}{(1+\exp(-2u))} - 1 \qquad (2-10)$$

$$\mathbf{h} = F(\mathbf{W}\mathbf{x} + \mathbf{b}) \qquad (2-11)$$

$$y = F(\mathbf{W_0}\mathbf{h} + b_0) \qquad (2-12)$$

where u is scalar variable, **x** is input vector $(P, Q)^T$, **W** is weight matrix of hidden layer, **b** is bias vector of hidden layer, **h** is hidden node vector, $\mathbf{W_0}$ is weight vector of output layer, b_0 is scalar bias of output layer, and y is target value (S).

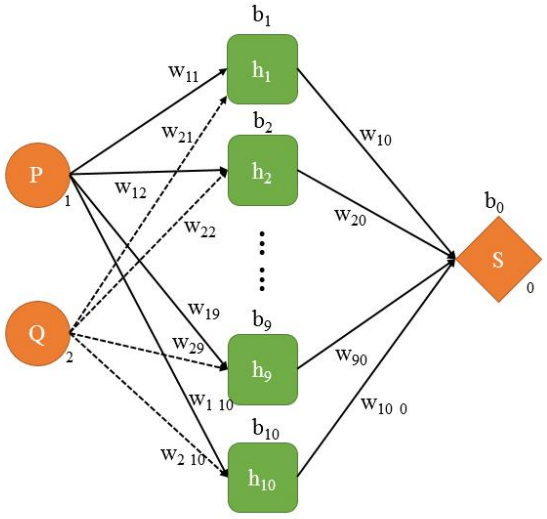

(a)

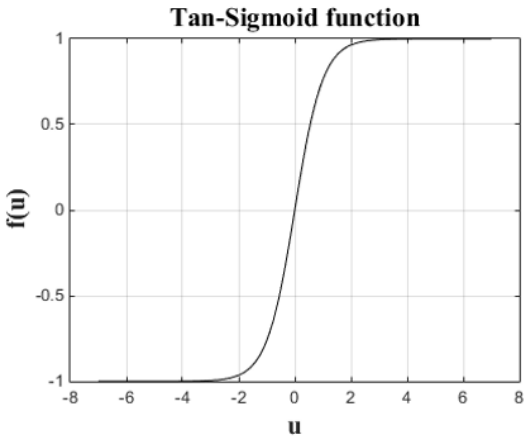

(b)

Figure 2-8. Artificial neural network : (a) schematic diagram; (b) Activation function

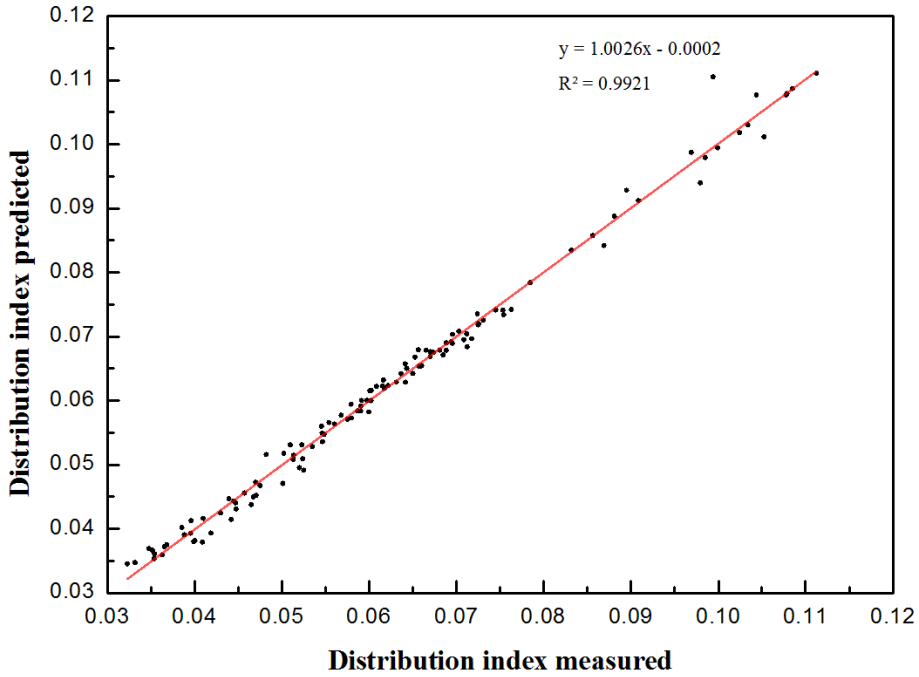

Figure 2-9. Comparison of the measured value and predicted values of distribution index

Fitting result of total data with respect to the training set 80%, validation set 10%, test set 10% is gained with 0.9921 of R-squared value shown in Figure 2-9. It can well predict the points near optimal in that the data is calculated with concentrated on the points near presumed optimal. The optimization is conducted for uniform distribution using 'fmincon' solver code in Matlab® 2014b with generated ANN function and optimal is on Table 2-5. P_{opt} and Q_{opt} are near the middle of feasible range and the uniform flow over the all main channels is achieved as presented in Figure 2-10a. The optimal function value and normalized distribution of S_{opt} is improved with compared to one of well-designed A-B-F-D guiding fin by 0.008 shown in Figure 2-10b. Both P and Q length are extended more by 1.97 and 7.89 mm than the A-B-F-D case. It is known that increased Q influences to carry a little more flow for the distribution near channel position 110, and the flow near channel position 1 is decreased by prolonged P.

Table 2-6 shows the comparison to previous research with present optimal design performance. For the microchannel device with more than 30 channels, the distribution performance of present study is the most improved one even though the simple guiding fin is introduced, the device size is much larger and it has more than 100 channels which is considered large scale.

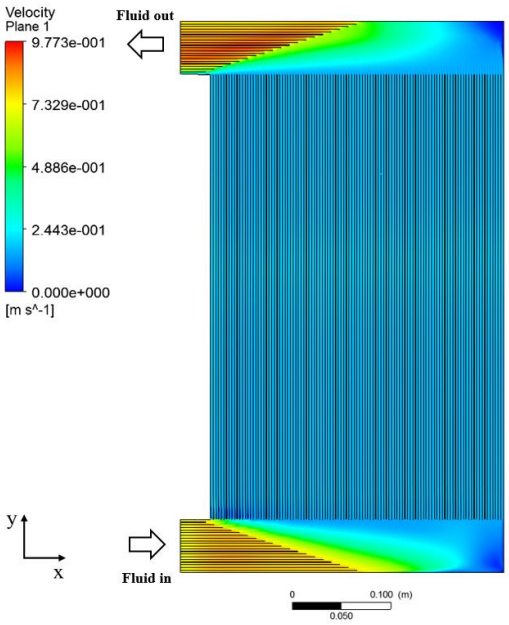

(a)

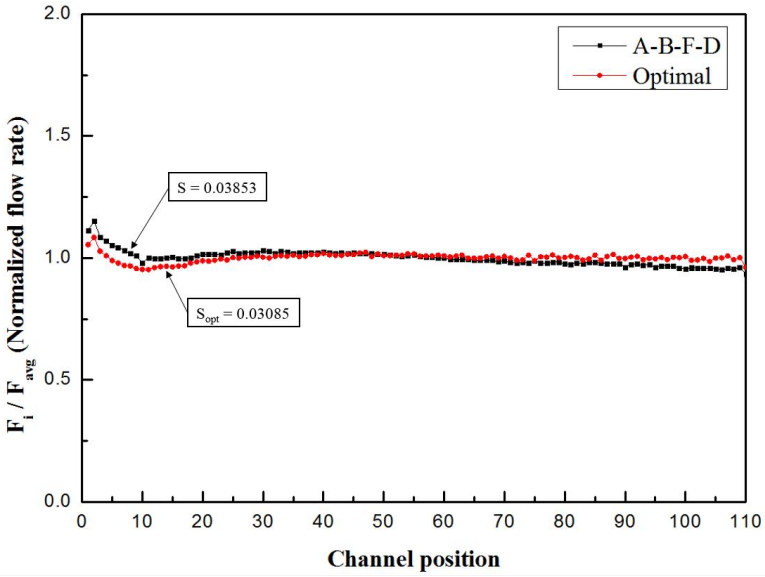

(b)

Figure 2-10. Velocity contour of optimal design (a), and normalized flow distribution of optimal and A-B-F-D geometry (b)

Table 2-5. Optimization result

Variable	Value
P_{opt}	16.97
Q_{opt}	185.89
S_{opt}	0.03085

Table 2-6. Comparison of present optimal design with previous study over 30 channels

	Previous study 1[15]	**Previous study 2[16]**	**Present study**
Total main channel number	68	30	110
Channel dimension Height / Width / axial length (mm)	0.25 / 0.394 / 31	6.5 / 2 / 250	3.05 / 2.6 / 450
Optimized distribution index	0.048	0.058	0.03085

2.5. **Robustness test**

The distributor typically has to be made robust with the variance of operating condition to be widely used in industry. In order to avoid the maldistribution from drastic change of operating condition, it is required to investigate the feasible range for uniform distribution. The main factors are the change of flowrate, fluid property from the exchange of coolant fluid or variance of temperature. They are highly related with Reynolds number (Re_{GF}) which is favorable to be estimated in inlet guiding channel since it well reflects the flow status influenced by the velocity of coolant inflow and viscous resistance at the border between the outlet of guiding fin and FMZ. Here, the feasible range is estimated with the variance of flowrate and fluid property for proposed optimal design.

2.5.1. Flowrate variance

In reality, there might be some variation of flowrate from the header to each coolant layer or heat removal performance is changed differently for the adjustment of the productivity. For sustainable operation, robustness on the flowrate change must be guaranteed. Table 2-7 shows the distribution index result for the flowrate range of 20 – 1000 % based on baseline flowrate 200 LPM and Re_{GF} is stated as well. There is a trend of increasing distribution index with deviated from the optimal (baseline flowrate). In case of flowrate increase, inertia force becomes larger than the viscous force with comparison to baseline. The flow

momentum out of guiding fin becomes larger. Fixed geometry of FMZ can't cover to make all the flow momentum changed. It leads to leaning of flow to channel position 110. As the same way, decrease of flowrate causes the maldistribution with focused flow near channel position 1 as the lower inertia momentum than baseline is fully changed before reaching channel position 110. Despite the slightly deviation of the distribution index from the baseline, robustness on the range 60 -1200 LPM which is under 0.058 considered uniform flow in literature[16] is achieved.

Table 2-7. Distribution index result with variance of flow rate of Syltherm 800 and corresponding Reynolds number of guiding fin

Factor	**Flow rate (LPM)**	**Re_{GF}**	**S**
20 %	40	364.6	0.06492
30 %	60	546.9	0.05640
50 %	100	911.6	0.04572
80 %	160	1458.6	0.03257
100 % (Base line)	200	1823.2	0.03085
120 %	240	2187.8	0.03216
200 %	400	3646.4	0.04187
400 %	800	7292.8	0.05358
600 %	1200	10939.2	0.05861
800 %	1600	14585.5	0.06150
1000 %	2000	18231.9	0.06455

2.5.2. Fluid property variance

For coolant fluid type change to be newly introduced, 4 types of coolant are tested on the optimal design in baseline condition. The distribution index result of Syltherm 800, Marlotherm N, Marlotherm SH, Dowtherm Q is presented in Table 2-8. Viscosity and density are mainly changed. All the coolant types are acceptable to be applied within uniform distribution range.

In case of temperature variation for operating condition change with sufficient margin, fluid property (density and viscosity) is changed in the same manner. Table 2-9 shows the performance with variance of temperature in the range of ± 80 ℃ deviation centered on baseline 230 ℃. It is assured that the uniform distribution is sufficiently guaranteed within given range.

In sum of robustness results, Figure 2-11 shows the distribution index with each type of variation in terms of log scale of Reynolds number in guiding fin. All three cases are overlapped with one line with symmetrically convex shape. It means the distribution trend is highly dependent on the Reynolds number in guiding fin and is related symmetrically with log scale of it. The uniform distribution is achievable within the Reynolds number range of 500 – 10800 under 0.058 of distribution index from the previous study[16]. Even in the Reynolds number of 1000-6000, proposed design shows more improved distribution performance than the previous best distribution index value, 0.048 in the literature[15] for large scale analysis. Thus, the optimal design is sufficiently considered robust geometry for distribution.

Table 2-8. Distribution index result with variance of fluid property (at 230 ℃) and corresponding Reynolds number of guiding fin

Fluid	**Density (kg/m^3)**	**Viscosity (Pa-s)**	**Re_{GF}**	**S**
Syltherm 800 (Baseline)	744.3	0.00081	1823.2	0.03085
Marlotherm N	736	0.00067	2179.6	0.03212
Marlotherm SH	894	0.00071	2498.3	0.03417
Dowtherm Q	806.6	0.00026	6155.4	0.05297

Table 2-9. Distribution index result with variance of temperature of Syltherm 800 and corresponding Reynolds number of guiding fin

Temperature (℃)	**Density (kg/ m3)**	**Viscosity (Pa-s)**	**Re_{GF}**	**S**
150	819.5	0.00170	956.5	0.04431
170	801.3	0.00139	1143.8	0.03851
190	782.8	0.00115	1350.5	0.03457
210	763.8	0.00096	1578.6	0.03117
230 (Baseline)	744.3	0.00081	1823.2	0.03085
250	724.2	0.00069	2082.6	0.03274
270	703.5	0.00059	2365.9	0.03306
290	682.0	0.00050	2706.5	0.03755
310	659.7	0.00044	2975.0	0.03806

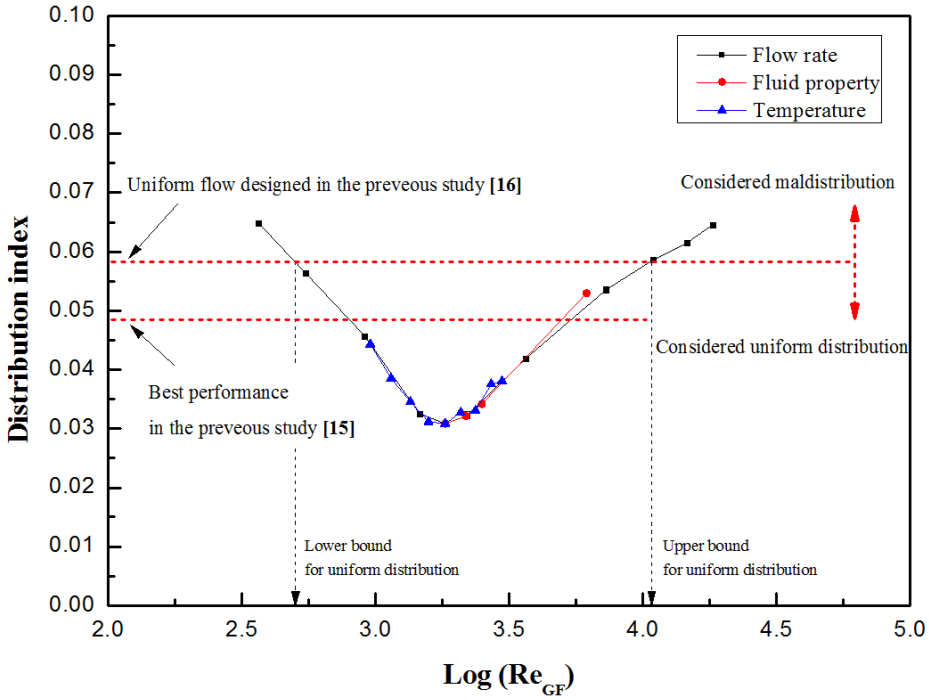

Figure 2-11. Reynolds number of inlet guiding fin vs. Distribution index for robustness tests

2.6. **Conclusions**

The trapezoidal-shaped simple guiding fin is introduced to achieve the uniform distribution in the U-type microchannel layer model with symmetric manifold geometry with 110 main channels. Turbulent mixing on the flow coming out from guiding fin outlet is made to change the flow momentum for main channel distribution. The geometry of FMZ directly related with the guiding fin shape mainly affects the distribution because the guiding fin plays a role of transporting fluid without momentum change. CFD based sensitivity analysis is conducted to identify the effect of the representative geometric variables, the upper and bottom length (P, Q) of guiding fin. Upper length locally affects the main channel distribution near inlet, whereas bottom one influences that far from inlet. Optimal design(P = 16.97, Q = 185.89) with 0.03085 of distribution index is obtained and made improvement by 0.01715 with compared to 0.048 of the current best in literature for large scale microchannel type layer. The uniform distribution for the optimal design is fully guaranteed on Reynolds number range of 500-10800, which means that robustness is identified. Proposed guiding fin distributor has the following advantages.

- ✓ Simple shape leading to ease of fabrication
- ✓ Guarantee of uniform distribution on large scale layer (over 100 channels) for ease of scale-up
- ✓ Distribution robustness made sure with additional region from

improved distribution performance for commercial use

CHAPTER 3: Optimal design of large scale microchannel Fischer Torpsch reactor module using Cell-coupling method

3.1. Background

Many studies on small gas-to-liquid (GTL) process for development of associate and stranded gas field.[1-3, 21-23] Modulization and compactness are important due to space limitation in that process. Especially, Fischer Tropsch synthesis(FTS) reaction is the main reaction but, highly exothermal reaction. The effective heat removal is required to achieve safe operation. Research on microchannel reactor with layers stacked fashion has been increasing for higher efficiency on heat removal than conventional reactors. It brings possibility to use more active catalyst since it can highly reduce the distance of heat and mass transfer in micro- to milli-scale. With the same production rate, the reactor volume can be reduced 10-1000 times than conventional reactors[4-6]. With small but high efficient reactor type, intensification and modularization of process deliver the higher efficiency and productivity[24-30]. In general, microchannel reactors are fabricated by layer stacking method and maintain regular arrangement due to ease of fabrication, structural bonding balance, and durability.

The most important goal in microchannel FTS reactor research is to find

conditions to keep the entire reactor isothermal to avoid hot spot. It is directly related with the operation safety. In single channel study, Giovanni Chabot et al. suggested the critical dimension of the tube diameter for runaway reaction in single channel fixed bed and the effects of tube diameter on seletivity and thermal performances[31]. Given conditions, the heat removal efficiency is highly affected form not the viscosity and heat capacity but thermal conductivity of gas mixture. Jens Knochen et al. presented 1 m capillary channel fixed bed reactor model with the modified Ergun equation coefficient and effective liquid holup factor to validate with experimental data[32]. They analyzed the effect of both channel width and proper catalyst size to avoid runaway reaction and, finally proposed the reactor scale-up design by numbering up the channels. Xiaowei Zhu et al. conducted the analysis of FTS heat transfer performance depending on types of catalyst support materials with reaction and without reaction[33]. They suggested performance with reaction increase 1.6~3.2 times more than that without reaction and the inherent conductivity of catalyst support material affect directly that of catalytic bed.

In multi-channel reactor study, computational fluid dynamics (CFD) is mostly used for heat, mass and momentum transfer analysis. Azarmandi et al. provide the positive effect of buoyancy with 2 phase boiling water as a cooling medium for intensification of FTS heat transfer performance using CFD[7]. Kshetrimayum et al. compare the heat removal performance among 3 types of cooling medium (cooling oil, subcooled water, and 2 phase saturated water) with catalyst loading changed[34]. Shin et al. modelled compact modular multi channel reactor using CFD and

investigate cooling performance in variation of coolant flowrate, location of process channels, and reactor seris[35]. CO conversion was increased with the number of process channels increased, but thermal runaway was sensitive to feed temperature change. Shin et al. presented the operation condition for reactor isothermal considering effect from ambient air heat transfer penetrated through the insulation material[9].

CFD, however, has limitations on anlaysis of multi-channel reactor with over 100 channels since it requires high compuational cost. In order to resolve this problem, Park et al. developed the Cell-coupling method for analysis of reactors over hundreds channels. Reactor model is decomposed many unit lumped cells, mass and heat balance is calculated with some flow path technic[12, 36]. It can consider the flow distribution, reactor configuration, all distributed parameters(mass, temperature, pressure, and velocity).

The design procedure for conventional way starts from single channel analysis step to that of multichannel. In single channel step, the critical dimensions like channel width, height, length, and thickness are chosen to achieve the target product rate, selectivity and to avoid hot spot, catalytic deactivation, high pressure drop. Then, it is numbering up to achieve target product rate under the well distributed momentum and heat transfer performance in multichannel step[37, 38]. This method is reasonable but, not close to optimal. It has some disadvantage that the main dimensions are determined in early stage phase like single channel analysis phase. In case of large-scale reactor, multi-channel analysis has limitation

that whole dimension conditions are not considered due to high computational cost in CFD analysis. Therefore, the whole reactor dimension with a given operation condition should be conceptually chosen through optimization the whole reactor considering reactor compactness and isothermality. There is no research on optimization of large scale microchannel reactor.

In this study, FTS microchannel reactor core with U-type cooling fashion was modeled using cell-coupling method for over 1000 channels and totally optimized for 7 design variables (Process channel height(PCH), cooling channel width(CCW), cooling channel height(CCH), the number of cooling channels matching with neighboring process channel(P_{Div}), the number of process channels on single layer(P_{Num}), the ratio of the number of process channel to the number of guiding channels in single layer(MR), the number of core cells along process channel flow direction($nj_{,core}$)). The objective functions are reactor core volume and maximum process channel temperature rise related with reactor compactness and operation safety respectively. The parameter sensitivity analysis for Coolant flowrate and 4 fixed design parameters(guide bar width(GBW), guide seam interval(GSI), outer shell thickness(OST), plate thickness(PT)) is conducted to measure the effect on the compactness under the same isothermality for each Pareto optimal. It is important for decision making of reactor design when what parameter we should modify with minimum loss of reactor strength for fabricator.

3.2. **Problem Description**

The conceptual module of compact FTS microchannel reactor is shown in Figure 3-1a. Syngas flows vertically down. Coolant flow into the bottom header and flow up and out from the same side of the inlet along U-type configuration. Figure 3-1b indicates a cooling layer at A-A'. Guide bar helps enhance the layer bonding and lay out a coolant flow path. There are guiding fins for well-distribution at inlet and outlet manifold as symmetry and main fins consisting of channels. To describe the inside reactor geometry, Figure 3-1c shows B-B' slice. Process and coolant layers are staked one by one. Between two layers, plate is inserted and outer shell plate is covered whole outer area.

The domain of the reactor is composed of process layers, cooling layers, outer shell, guide bar, plate, and seam except for headers in Figure 3-1a. Seam with the same width of single process channel is inserted at middle of both layers along the direction of flowing syngas and bonded to enhance inner layer. Target production rate is C_{5+} 0.5 BPD. Syltherm 800 in silicone type oil is used as cooling medium due to high stability on -40 to 400 ℃ and durability. In order to keep the temperature difference between inlet and outlet coolant lower than 1 K, coolant flow rate is sufficiently set as 500 LPM in base case. Inlet temperature of syngas and coolant is 220 ℃ for stable reaction.

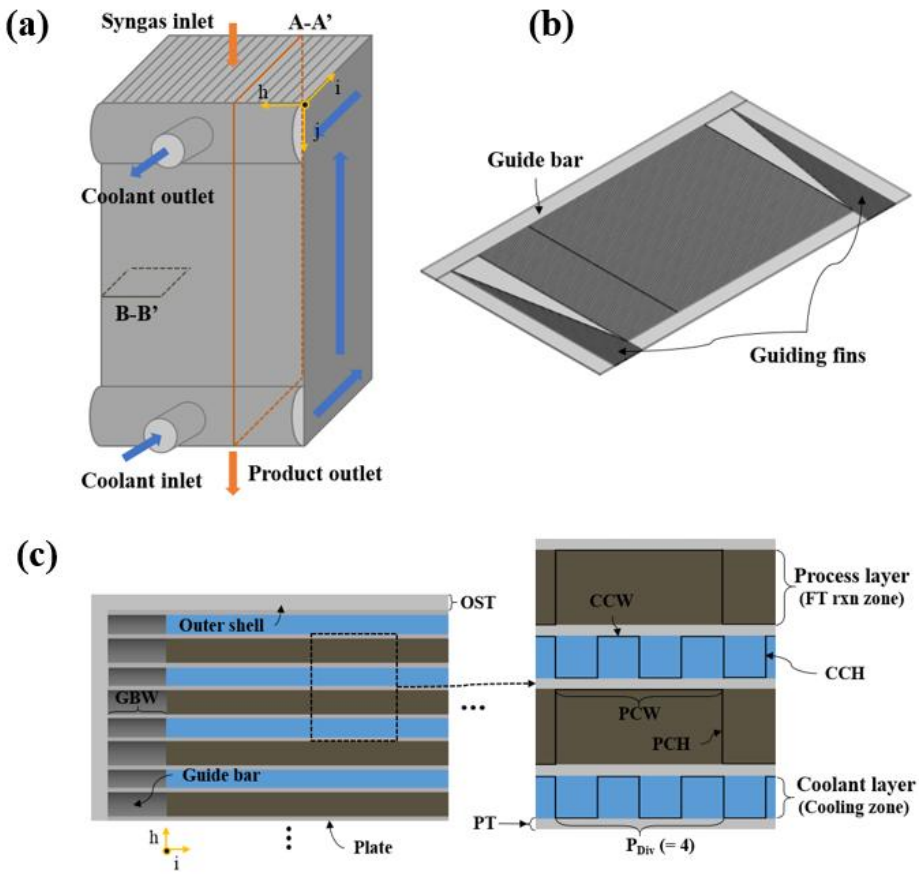

Figure 3-1. Conceptual geometry of compact Fischer-Tropsch reactor: (a) entire reactor core, (b) single cooling layer at A-A', (c) inside reactor geometry at B-B'

Overall work flow of present study is shown in Figure 3-2. Multi-objective optimization for C5+ 0.5 BPD compact FTS microchannel reactor model is conducted and sensitivity analysis of fixed geometry and operation parameter is studied. First of all, the distributed parameter reactor model is constructed using cell coupling method. No further validation is required in this study because the model already validated from Park et al.[36]. 11 model input are composed of 7 design variables, 4 fixed design parameters, and a operation parameter listed Table 3-1. Two main output are reactor core volume and $\Delta T_{max.}$ Seven design variables are used in core calculation of heat and mass balance and as optimization variables. The other parameters are just used in sensitivity analysis. In second step, multi-objective optimization is conducted for reactor core volume and $\Delta T_{max.}$ Minimizing reactor core volume increases reactor compactness and minimizing $\Delta T_{max.}$ brings reactor isothermal condition as safe operation and ease of performance controls like conversion, selectivity. If we have sufficient margin of ΔT_{max}, there is opportunity for process revamping[39]. To extremely reduce ΔT_{max} in given condition, channel dimension becomes smaller to make heat transfer distance short. Meanwhile, fabrication material is needed more due to much more channels are required. Pareto optimal can be obtained since two objective functions have trade-off relationship. Lastly, case studies for operation parameter and fixed design parameters are conducted. In coolant flow rate, we can obtain the proper value, that is, reject inefficient flowrate region under the same target production rate. Based on that flowrate, case study for4 fixed design parameter is carried out. Those are the

key parameter for reactor design durability and mutually related with each other. If parameters are too large, then reactor is not compact. Reversely, it is not durable with all low parameters. It depends on the fabrication capability of reactor production company. Therefore we should identify the quantitative effect of each parameter on the reactor core volume under the same ΔT_{max} Using that information, we can determine what fixed design parameter should be considered in priority.

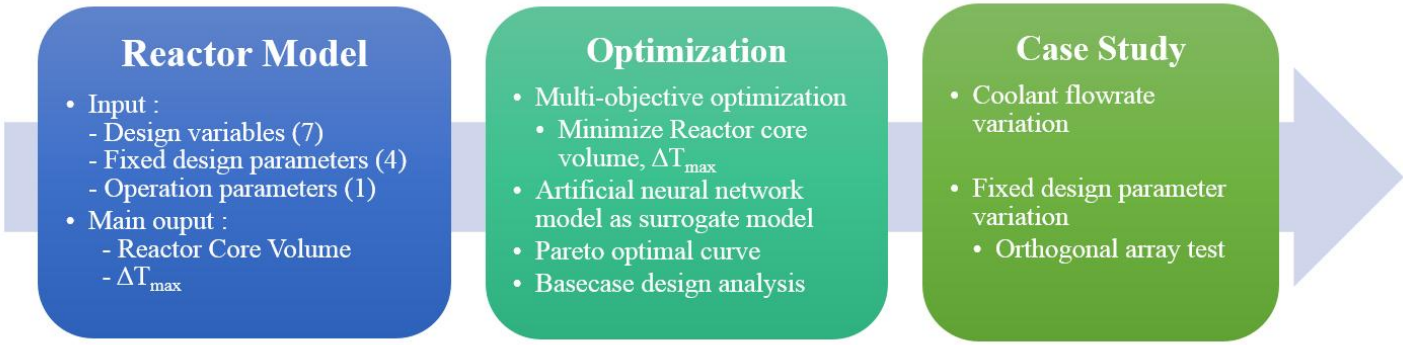

Figure 3-2. Overall work flow

3.2.1. Reactor Model description

The calculation domain for both reactor core layers is illustrated in Figure 3-3. In detailed, the green colored catalyst zone in process layer and the overlapped location in cooling layer.

Model input are 7 design variables, 4 fixed design parameters, 1 operation parameter as listed in Table 3-1. As illustrated in Figure 3-1c and Figure 3-3, PCH and CCH mean the height of process channel and cooling channel. CCW is the width of the cooling channel and is considered the dimension of unit cell for the cell coupling method. The width of guiding channels in guiding fin is even the same as CCW. P_{DIV} is the number of cooling channels matching with neighboring process channel. P_{Num} is the number of process channels on single layer. MR is the ratio of the number of process channel to the number of guiding channels in single layer. For example Figure 3-3(a) presents domain structure scheme with $P_{Div} = 4$, $P_{Num} = 12$, and MR = 2. $nj_{,core}$ is the number of core cells along process channel flow direction, which determines the core length. Given above 7 design variables, the reactor core model can be easily constructed.

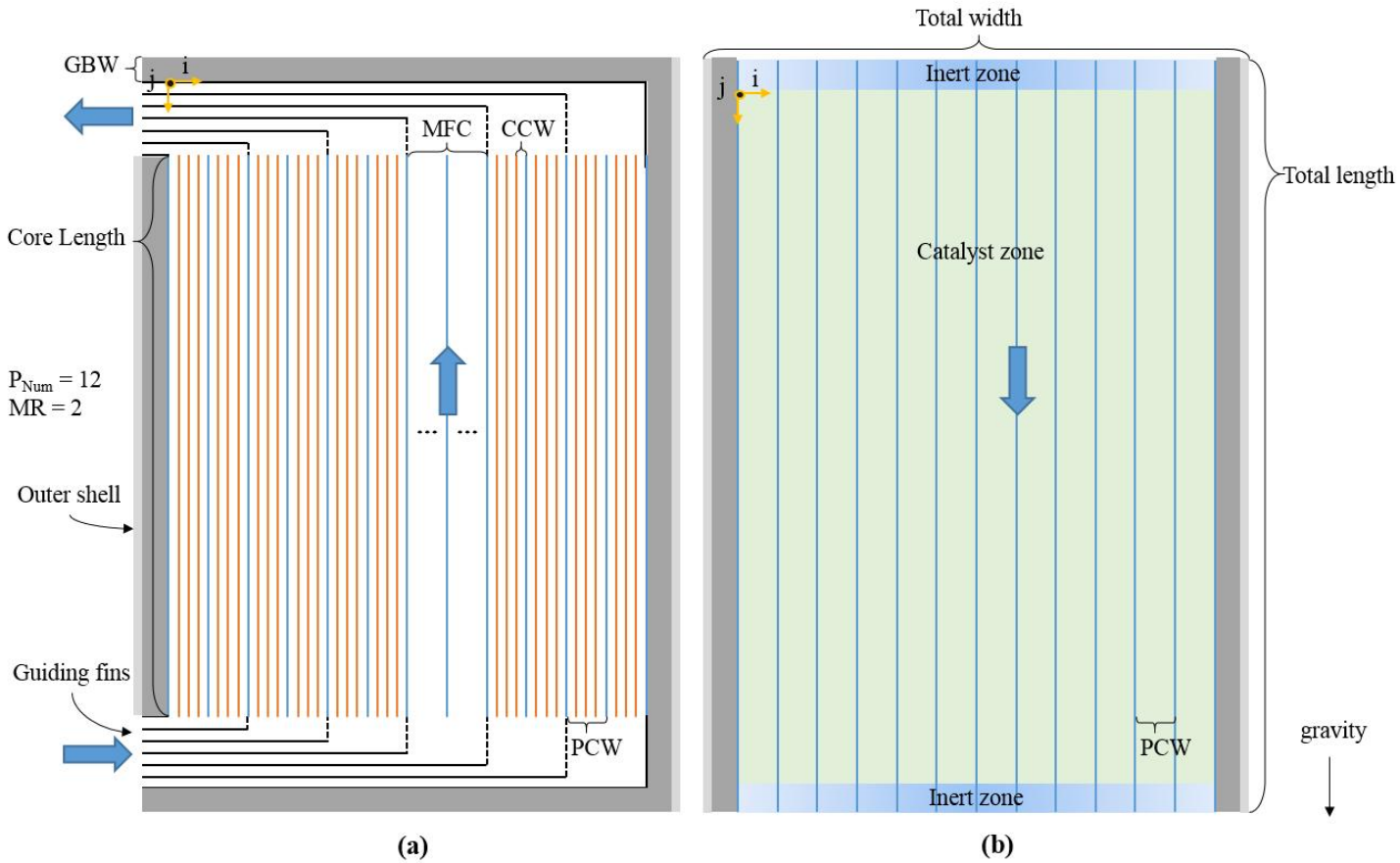

Figure 3-3. Layer domain structure scheme with P_{Div} = 4, P_{Num} = 12, and MR = 2: (a) Cooling layer, (b) Process layer

Table 3-1. Reactor system variables and parameters

Design variables	**Lower bound**	**Upper bound**	**Unit**	**Variable assignment**	**Variable type**
PCH	1	8	mm	x_1	Real
CCH	1	3.5	mm	x_2	
CCW	1.5	3	mm	x_3	
P_{Div}	2	5	-	x_4	Integer
P_{Num}	8	25	-	x_5	
MR	2	5	-	x_6	
$n_{j,\ core}$	70	385	-	x_7	
Fixed design parameters	Value				
GBW	30		mm	y_1	Real
GSI	120		mm	y_2	
OST	10		mm	y_3	
PT	1.2		mm	y_4	
Operation parameters	Value				
Coolant Flowrate	500		LPM	z_1	Real

In fixed design parameters, GBW is the width of guide bar. As it is increased, the bonding area between process and cooling layers becomes larger, which strengthen the reactor. GSI indicates the interval of guide seam. If the core width is larger than this value, the guide seam should be inserted. The guide seam along the process channel is inserted with the same dimension of process channel. It is important to enhance inner layer durability. OST means the thickness of outer shell. This shell covers entire the reactor to prevent the total swelling. PT is the thickness of the plate between layers. It averts the layer swelling. All 4 parameters mutually works each other to enhance the reactor durability. Additional dimension can be expressed using above design variables and parameters as follows:

$$\mathrm{PCW} = \mathrm{CCW} \cdot \mathrm{P_{Div}} \qquad (3-1)$$

$$\text{Core length} = \mathrm{n_{j,core}} \cdot \mathrm{CCW} \qquad (3-2)$$

$$\text{Total length} = \text{Core Length} + 2\left(\frac{\mathrm{P_{Num}}}{\mathrm{MR}} \cdot \mathrm{GBW}\right) \qquad (3-3)$$

$$\text{Total width} =$$

$$2 \cdot (\mathrm{GBW} + \mathrm{OST}) + \mathrm{PCW} \cdot \mathrm{P_{Num}} + \mathrm{PCW} \cdot \mathrm{floor}\left(\mathrm{PCW} \cdot \frac{\mathrm{P_{Num}}}{\mathrm{GSI}}\right) \qquad (3-4)$$

Core algorithm used in present study follows cell coupling method developed from park et al. [36]. Mass and heat balance equation are shortly expressed in Table 3-2. Revised point is that n_h is newly updated to achieve target product rate, 0.5 BPD using external iteration loop.

U-type microchannel reactor is decomposed into unit cells cut by j-, i-, and h-

direction for to apply cell-coupling method as illustrated in Figure 3-4. Green colored cells indicate the ones in the cooling layer and gray one is process layer. Noted γ_s^t is flow path pointer for t-th cell on flow path s presented in Eq(6). Dashed edge cells are ideal cell readily to understand. Whole coolant cell are linked by γ_s^t. Inlet coolant flow distribution is assumed to be uniform. It is readily achieved by proper header and manifold guiding fins[15, 20, 40-42].

For CO consumption rate, Langmuir-Hinshelwood type equation proposed by Yates and Satterfield is used as lumped kinetics model as follows[43]:

$$-\mathrm{r}_{CO} = \frac{k_0 \exp\left(-\frac{E_a}{RT}\right) {P_{CO}}^a {P_{H_2}}^b}{(1 + cP_{CO})^2} \qquad (3-8)$$

FTS catalyst is 12 wt% Co catalyst supported on γ-Al_2O_3 prepared by impregnation method. The kinetics model is Valid on the operation temperature region 220~240℃ with $R^2 > 0.9765$. Kinetic parameters are listed in Table 3-3.

Table 3-2. Cell based heat and mass balance equation for cell coupling method

Equations	**Remarks**
$\mathrm{Q}(j,i,h) - \sum_{\lambda}\sum_{\mu}\sum_{\nu}\left[\mathrm{U}(\lambda,\mu,\nu)\cdot A\cdot\{T_p(j,i,h) + (-1)^u\cdot T_p(\lambda,\mu,\nu) + (-1)^q\cdot T_c(\lambda,\mu,\nu)\}\right] = 0 \quad (5)$	Energy balance for reactant flow in process channel cells
Heat transfer in fluid: $\mathrm{m_c}(\gamma_s^t)\cdot C_p\cdot T_c(\gamma_s^t) = m_c(\gamma_s^{t-1})\cdot C_p\cdot T_c(\gamma_s^{t-1}) + +\sum_{\lambda}\sum_{\mu}\sum_{\nu}\left[U(\lambda,\mu,\nu)\cdot A\cdot\{T_c(\mathrm{j,i,h}) + (-1)^u\cdot T_p(\lambda,\mu,\nu) + (-1)^q\cdot T_c(\lambda,\mu,\nu)\}\right] \quad (6)$	Energy balance for coolant flow along γ_s flow path cells

where Q is heat generation [kW], U is the overall heat transfer coefficient [kW/m^2-K], A is characteristic area for the heat transfer [m^2], T_p is the temperature in the process channel cell [℃], T_c is the

temperature in the cooling channel cell [℃], m_c is the coolant flow rate [kg/s], and C_p is the heat capacity of the coolant [kJ/kg-K]. The u and q in the exponent of (-1) is used to describe the direction of the heat flow.

$$\mathrm{F_s(j,i,h)} = \mathrm{F_s(j-1,i,h)} + \rho_{cat} \cdot V_{element} \cdot \sum_{w} \nu_{sw} \cdot r_w \qquad (7)$$

Mass equation	where $\mathrm{F_s}$ is the molar flow rate of component s [mol/s], ρ_{cat} is bulk catalyst packing density [kg/m^3], $\mathrm{V_{element}}$ is the volume of unit cell [m^3], ν_{sw} is the stoichiometric coefficient of component s in reaction w, and $\mathrm{r_w}$ is the reaction rate [mol/kg$_{cat}$-s].	Mass balance for reactant flow in process channels

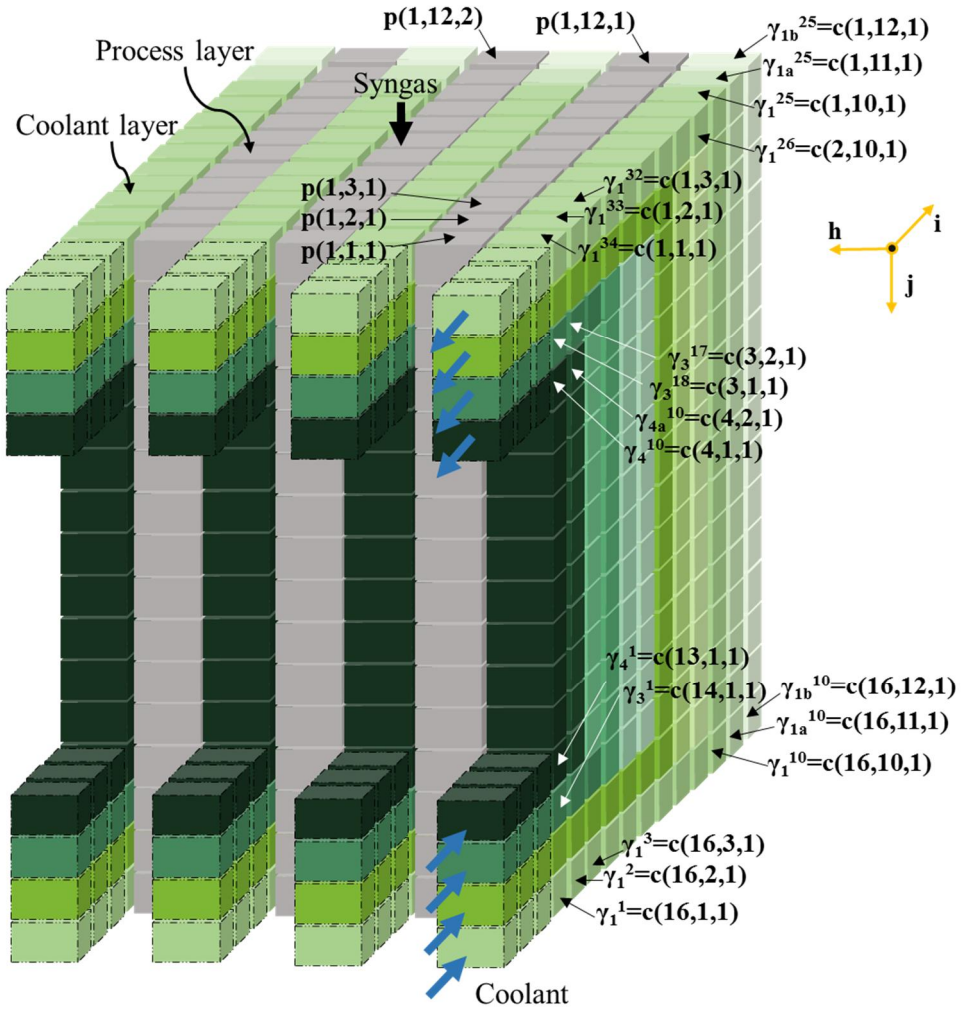

Figure 3-4. Cell domain example and flow path construction for cell coupling model into U-type FTS microchannel reactor ($n_{j,\,core}$ = 8)

Table 3-3. Lumped FTS kinetic parameters for Eq. (3-8)

k_0	E_a	a	b	c
5.0 x 10^7	95	0.50	0.50	0.30

Reactor core volume is calculated using n_h after the end of revised reactor simulation and The other main output, $\Delta T_{max,}$ is calculated as follows:

$$\text{Total height} = (n_h + 1) \cdot (CCH + 2 \cdot PT) + n_h \cdot PCH + 2 \cdot OST \quad (3-9)$$

$$\text{Reactor Core Volume} = \text{Total length} \cdot \text{Total width} \cdot \text{Total height} \quad (3-10)$$

$$\Delta T_{max} = \max(\forall T_p) - \text{Inlet Temperature} \quad (3-11)$$

3.2.2. Reactor model validation

The experiment of pilot scale microchannel FT reactor was conducted in KOGAS as shown in Figure 3-5. The detail experimental data and reactor geometry was not presented in this thesis due to company internal confidential. The only validation result was illustrated in Figure 3-6. The CO conversion and temperature in process channel of the reactor model is validated within feasible range of interest. It shows less than 7% relative error. The used catalyst was the same one the kinetics of which was stated in Eq (3-8). Target production rate was C_{5+} 0.5 BPD.

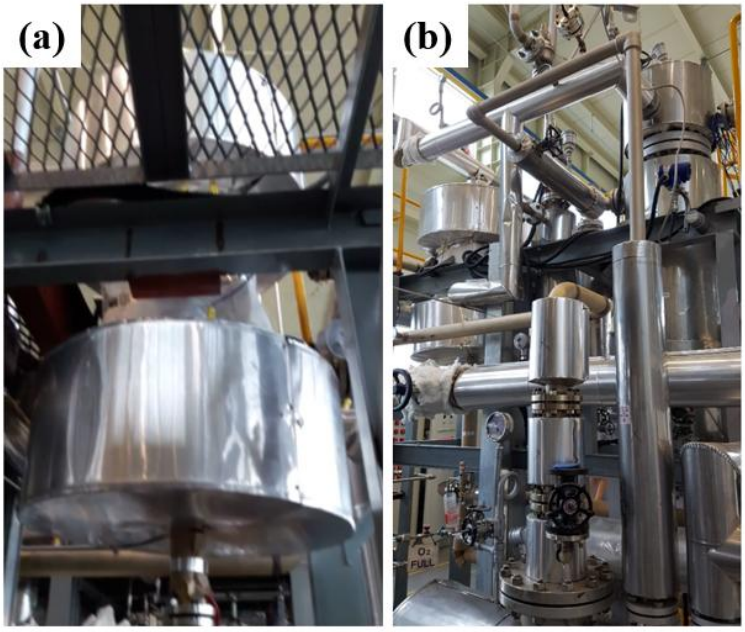

Figure 3-5. KOGAS FT reactor experimental setup : (a) Insulated microchannel FT reactor, (b) FTS process

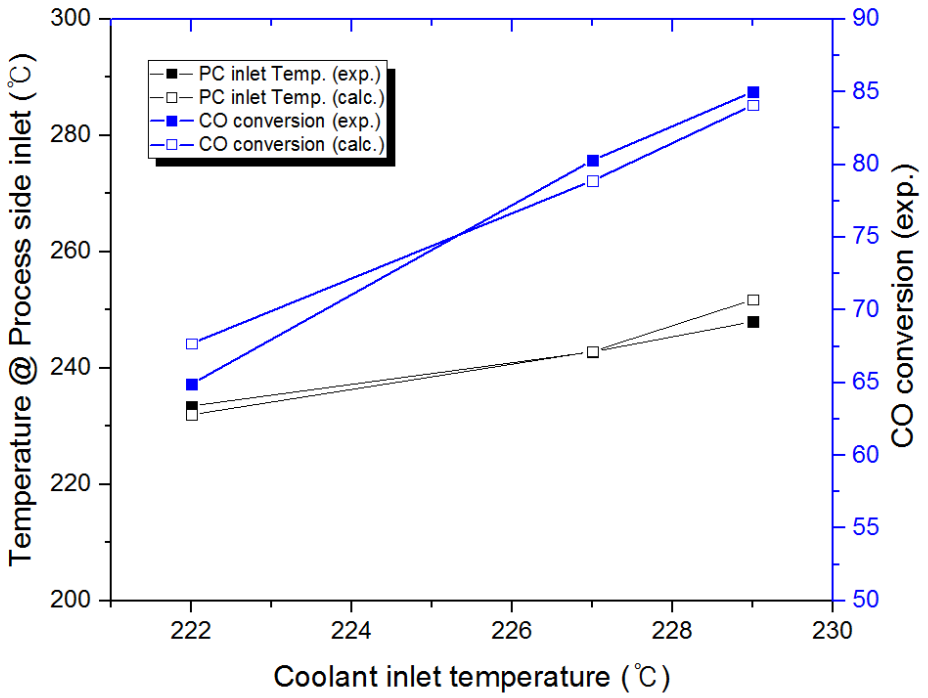

Figure 3-6. Comparison of reactor model calculated data and experimental measured data

3.2.3. Optimization methodology

Main purpose of multi-objective optimization is to obtain pareto optimal curve based on the trade-off relationship between reactor core volume and ΔT_{max} for 7 design variables. Characteristic of them is mixed integer variable, $x(\in \mathbb{R}^3 \times \mathbb{Z}^4)$. Then, we can define the searching area S of x based on the lower and upper bound in Table 3-1. Let other input parameters put $y(\in \mathbb{R}^4)$ as fixed design parameters and $z(\in \mathbb{R})$ as operation parameter. We can define f_{yz} $(: \mathbb{R}^3 \times \mathbb{Z}^4 \longrightarrow \mathbb{R}^2$, where $f_{yz1}(x)$: Reactor core volume , $f_{yz2}(\boldsymbol{x})$: ΔT_{max} @ specific $\boldsymbol{y}, \boldsymbol{z})$ as reactor model based specific y and z. The mixed integer nonlinear programming optimization can be formulated as follows:

$$
\begin{aligned}
&minimize\ [f_{yz1}, f_{yz2}] \\
&\text{s. t.} \\
&\boldsymbol{x} \in \boldsymbol{S} \\
&\text{Total width} < \text{Total length} \\
&\text{Total height} < \text{Total length} \qquad (3-12)
\end{aligned}
$$

Loose dimension constraints are included for ease of fluid distribution. Reactor model is highly complicated and nonlinear, so that derivative-free method should be used. If partially total simulation is conducted as $\boldsymbol{x}$ as all integers, the number of simulations is over 5 million times. Surrogate model based optimization is needed because multi-objective optimization requires many optimal points for pareto curve. In this study, artificial neural network(ANN) generated by set of

randomly selected simulation points. Especially, integer type variable of P_{Div}, P_{Num}, MR, and $n_{j,core}$ are relaxed and considered as real type variables to make problem hold low computational load by nonlinear programming(NLP). NLP optimal should be converted to original variable type through rounding operation for integer type variable. Used NLP solver is MINOS in GAMS Distribution 24.7.2. Sufficient numbers of optimization with random initial point set are carried out to supplement the initial point dependency of local solver, MINOS.

ANN is widely used for highly nonlinear function fitting. For compensation of the scale difference, normalization processes to all design variables and function model values by using upper and lower bound. Then, normalized design variables and function values(reactor core volume and ΔT_{max}) are assigned as inputs and target variables. Data points are allocated to training set 70%, validation Set 15 %, test set 15%. For high prediction accuracy, ANN function has 14 hidden nodes with $R^2 > 0.99$. Figure 3-7 illustrates the ANN schematic diagram used in present study. Tan-sigmoid function is used as activation function as written below.

$$F(u) = \frac{2}{(1+\exp(-2u))} - 1 \qquad (3-13)$$

$$\mathbf{h} = F(\mathbf{wx} + \mathbf{b}) \qquad (3-14)$$

$$\mathbf{y} = F(\mathbf{Wh} + \mathbf{B}) \qquad (3-15)$$

where u is scalar variable, **x** is input vector, **w** is weight matrix of hidden layer, **b** is bias vector of hidden layer, **h** is hidden node vector, $\mathbf{W_0}$ is weight vector of output layer, **B** is bias vector of output layer, and **y** is target vector.

where u is scalar variable, **x** is input vector, **w** is weight matrix of hidden layer, **b** is bias vector of hidden layer, **h** is hidden node vector, $\mathbf{W_0}$ is weight vector of output layer, **B** is bias vector of output layer, and **y** is target vector.

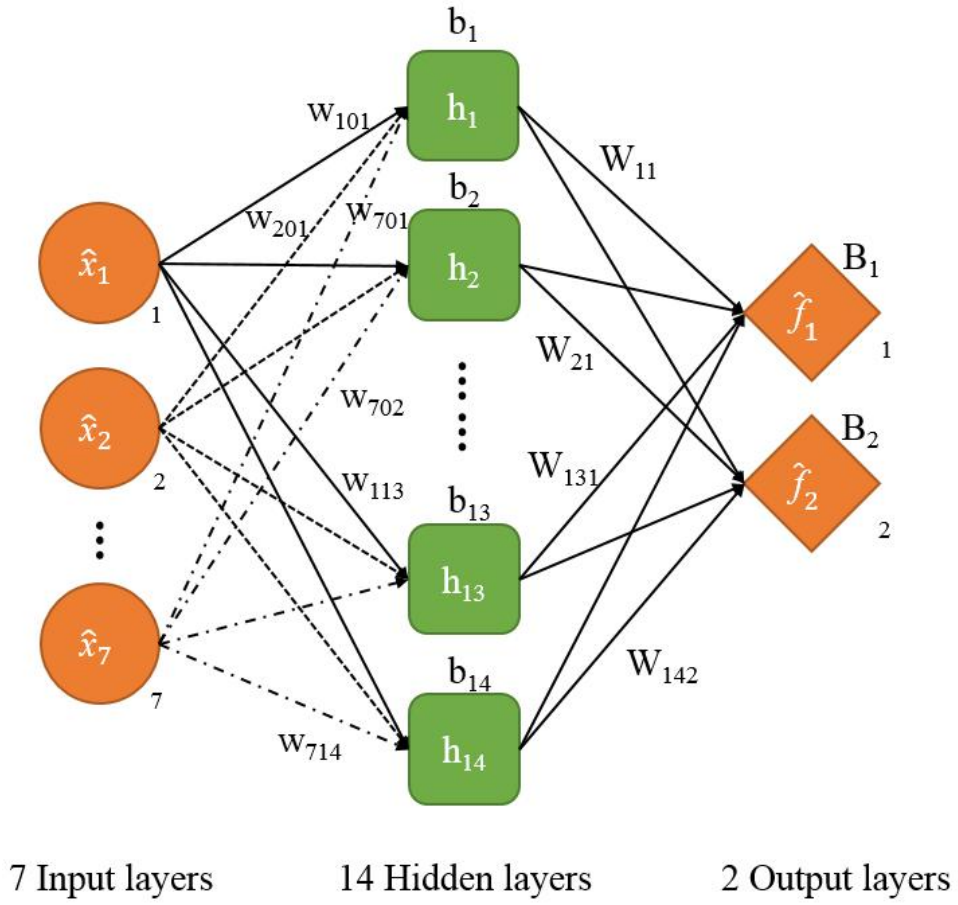

Figure 3-7. Schematic diagram of artificial neural network

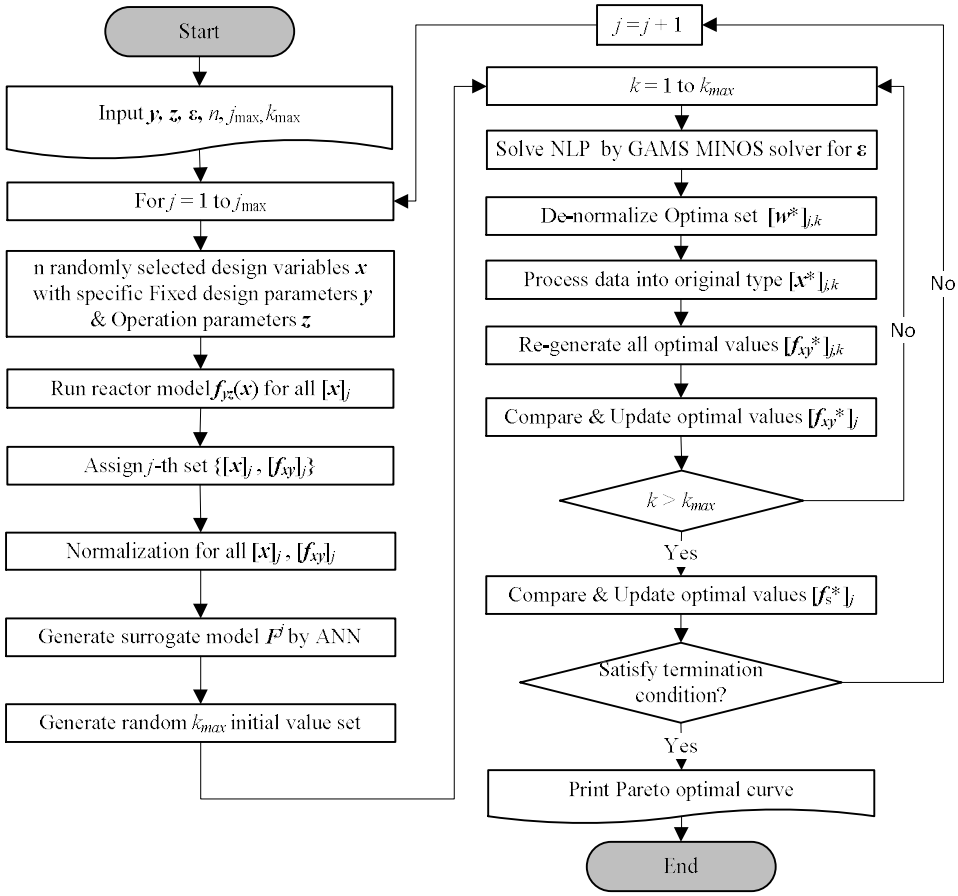

Figure 3-8. Multi-objective optimization procedure using surrogate model

Figure 3-8 shows the overall procedure of multi-objective optimization using ANN as surrogate model. Firstly, parameter set $\boldsymbol{y}$, $\boldsymbol{z}$, user defined ε set for epsilon-constraints method, n(the number of sets for design variable $\boldsymbol{x}$), j_{max}(the maxmum number of n random data selection), k_{max}(the number of initial value sets) are input. In j-th n data selection step, n design variable data are randomly selected for ANN formation. Let n-randomly selected design variable set put $[\boldsymbol{x}]_j \in \mathbb{R}^{n\times 7}$ and their function value set put $\left[\boldsymbol{f_{yz}}\right]_j \in \mathbb{R}^{n\times 2}$ based on specific $\boldsymbol{y}$, $\boldsymbol{z}$. Then, j-th set can be defined as $\left\{ [\boldsymbol{x}]_j, \left[\boldsymbol{f_{yz}}\right]_j \right\} \in \mathbb{R}^{n\times 9}$. After normalization of j-th set, ANN is generated. Let ANN surrogate model define $\boldsymbol{F^j}(:\mathbb{R}^7 \longrightarrow \mathbb{R}^2$ where F^j_1 : Predicted normalized reactor core volume, F^j_2 : Predicted normalized ΔT_{max}) and optimization variable set put $\boldsymbol{w} \in \mathbb{R}^7$. Multi-objective optimization NLP problem can be solved by applying ε-constraint method as follows[44]:

$$Minimize\ F^j{}_1(\boldsymbol{w})$$

$$s.t.\ 0 \le w_i \le 1 \quad (i = 1..7)$$

$$\text{Total width} < \text{Total length}$$

$$\text{Total height} < \text{Total length}$$

$$F^j{}_2(\boldsymbol{w}) < \varepsilon_p\ , \qquad where\ p = 1, 2, .. \qquad (3-16)$$

This optimization procedure composed of two iteration loops. Inner loop take the optimization of $\boldsymbol{F^j}$ generated single j-set using k_{max} sets of random initial points. In outer loop, optimization of $\boldsymbol{F^j}$ is attained to keep j-set changed to obtain final pareto optimal curve. For compensation of initial point dependency for local NLP solver,

k_{max} sets for initial points are selected for single *j*-set. NLP problem defined as ε-constraint formulation is solved using MINOS for all $\boldsymbol{\varepsilon}$ elements(ΔT_{max} constraint). Normalized optimal set $[\boldsymbol{w}^*]_{j,k}$ is obtained. It needs to be processed for de-normalization and de-relaxation into original variable type $[\boldsymbol{x}^*]_{j,k}$ and save $[\boldsymbol{f}^*_{\boldsymbol{yz}}]_{j,k}$ with applying to original reactor model. Inner iteration takes k_{max} times, and $[\boldsymbol{f}^*_{\boldsymbol{yz}}]_j$ is acquired by gathering the optimal values of each ε_p class with comparing all $[\boldsymbol{f}^*_{\boldsymbol{yz}}]_{j,k}$. The total number of optimizations is k_{max} times the number of $\boldsymbol{\varepsilon}$ elements for sinlge *j*-set. In specific *j*-th iteration, $[\boldsymbol{f}^*_{\boldsymbol{yz}}]_j$ is compared with $[\boldsymbol{f}^*_{\boldsymbol{s}}]_{j-1}$ in each of $\boldsymbol{\varepsilon}$ element. Advanced values are updated on $[\boldsymbol{f}^*_{\boldsymbol{s}}]_j$ and the rest values of $[\boldsymbol{f}^*_{\boldsymbol{s}}]_{j-1}$ are allocated on the vacancies. If there is no update, $[\boldsymbol{f}^*_{\boldsymbol{s}}]_j$ is printed as the pareto optimal.

3.2.4. Case study

Two case studies are carried out to clarify the effect of parameters on the pareto optimal: Coolant flowrate as operation parameter and 4 fixed design parameters.

For coolant flowrate variation, 5 cases are generated within 350 ~ 1500 LPM to keep the fixed design parameter unchanged including base case (500 LPM) as listed in Table 3-4. The main purpose of this case study is to exclude the inefficient coolant flow rate region by comparing with each pareto optimal curve.

Nextly, influences of the variation of fixed design parameters on the pareto optimal need to be analyzed. Each characteristic of four fixed design parameters is

obvious positively or negatively. They, however, are mutually related directly to the geometric stress with durability. We should identify which parameter should consider first priority in quantitative balanced influence. Those are required to be determined though the discussion with fabrication company.

Table 3-4. Case list for various coolant flow rate

	Fixed Design Parameter				**Operation Parameter**
Case No.	GBW (mm)	GSI (mm)	OST (mm)	PT (mm)	Coolant flowrate (LPM)
Base					500
1					1500
2	30	120	10	1.2	1000
3					750
4					300

Table 3-5. Two level of fixed design parameter

Parameter	GBW	GSI	OST	PT
L1	15	60	10	0.6
L2	30	120	20	1.2

Each parameter has two level with approximately equal size effect on the reactor as shown in Table 3-5. The one-dimensional influence of each effect can be analyzed when 2^4(=16) cases are generated. In this part, economical $L_8(2^7)$ orthogonal array test that is widely used in degree of experiments field is applied for reduction of processing time. According to that method we can set 8 experiments that is half of total testing. The balanced effect of each parameter is distributed to all cases listed in Table 3-6. Every case has orthogonal relation with each other. Analysis of variance should be conducted to estimate the effect of each parameter by setting 'No effect to result' as null hypothesis.

Table 3-6. Case study list for L8(27) Orthogonal Array

	Fixed design parameter				**Operation parameter**
Case No.	GBW (mm)	GSI (mm)	OST (mm)	PT (mm)	Coolant flowrate (LPM)
1	15	60	10	0.6	
2	15	60	10	1.2	
3	15	120	20	0.6	
4	15	120	20	1.2	
5	30	60	20	0.6	500
6	30	60	20	1.2	
7	30	120	10	0.6	
8 (Basecase)	30	120	10	1.2	

3.3. **Results and discussion**

The detailed analysis for the pareto optimal of base case is carried out to attain the various characteristics. Then, the case studies explained above are conducted for parameters. The operation condition of every case is in Table 3-7.

3.3.1. Base case

Figure 3-9 presents the pareto optimal curve of base case. Sixteen red dots indicate the pareto optimal from **ε** set of 3.8 to 6.8 K with the interval of 0.2 K. It can be considered within the isothermal status. Isothermal criteria in present study follows ΔT_p (Temperature difference of maximum and minimum in catalytic bed) < 4 K that sufficiently tight thermal control can be achieved. '+' signs present arbitrary j-set consisting of corresponding function values of 1500 randomly selected design variables. sky colored circles exhibit model function values calculated from 30000 randomly selected design points to check out whether the final results are Pareto curve or not. Pareto optimality has the important points as follows: 1) We can choose the design with the lowest ΔT_{max} with reactor volume fixed. It means the reactor design with more stability and controllability can be selected. 2) Decisions regarding a more compact design with ΔT_{max} fixed can be made.

Table 3-7. Operation conditions

Space velocity	4000	ml/g_{cat}-hr
Catalyst bed density	744.3	kg/cum
H_2:CO:N_2 ratio	64:32:4	-
Syngas feed temperature	220	℃
Coolant inlet temperature	220	℃

Figure 3-9, 3-10 show the model function values and process temperature distribution diagram of 3 representative optimal designs for ε = 3.8, 5, and 6.2 K. The maximum temperature point occurs near the inlet position of syngas in all points. Optimal reactor volume of ε = 3.8 K is 1.38 times larger than that of ε = 6.2 K. Detailed optimal data is listed in Table 3-3. Remarkable feature is that the length of reactor becomes shorter as ε increases. Meanwhile, the width and height exhibit not much variated. As ε increases, PCH increases, but it shows the optimal between both bound and CCH of all points presents the lower bounds. It means it depends on the capability of the fabrication company. P_{Num} shows the values around maximum. It depends on MR. CCW and P_{Div} has the optimum between bounds.

Cross sectional areas normal to j-direction depending on ε from single channel to single layer and whole reactor of process and cooling side is plotted in Figure 3-11. All areas related with process channels are gradually increased like that the PCH . Meanwhile, those of cooling channels shows the certain constant values except points of ε = 3.8 and 4.4 K. The reason is that it strongly depends on n_h value with constant CCH. Decreasing reactor length comes from increasing the cross sectional area of whole reactor process channels. This results in a relatively low heat transfer area per volume and conversely ΔT_{max} rises. Within a temperature range where thermal control is possible, a small rise in temperature leads to a slight increase in reactivity, which can increase productivity. It can lead to shortening reactor length.

If the baseline reactor was set as the same volume as referred design in Section

3.2.2 and is fixed at the upper bound of the isothermal condition (ΔT_{max} = 6.8 K), the optimal design with the same volume can be obtained with 40% reduced (ΔT_{max} = 4 K). In addition, a reactor design that can be miniaturized by 27% can be derived at the same level of ΔT_{max}. The selected optimal design depends on the process design specification set by the user, but in general, the best design can be chosen between the points of e = 4 to 4.6 K, which are closest to the origin in the Pareto curve.

From another point of view, ΔT_p < 5 K was sufficiently satisfied when deriving kinetic constant value and the KOGAS single channel reactor. However, due to the additional thermal effect occurring in the multichannel reactor, the multichannel reactor had ΔT_p exceeding 6 K. This proves that the optimal design obtained from a single channel cannot be in the multichannel reactor.

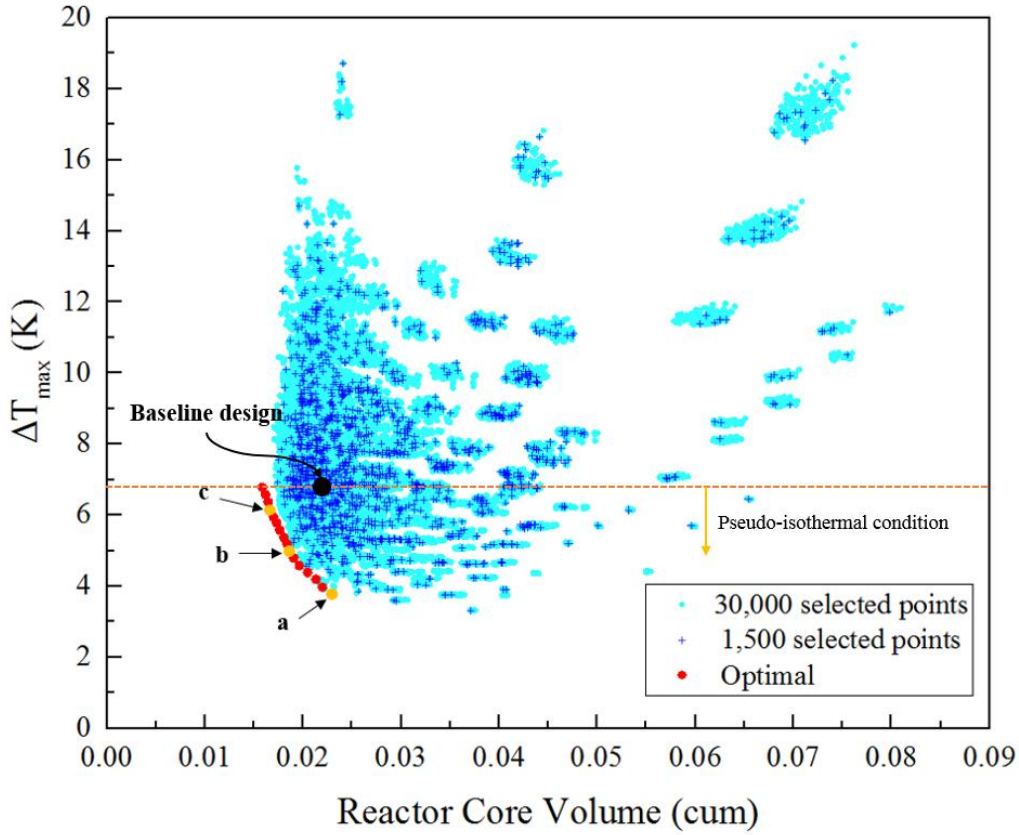

Figure 3-9. Base case optimal Pareto curve

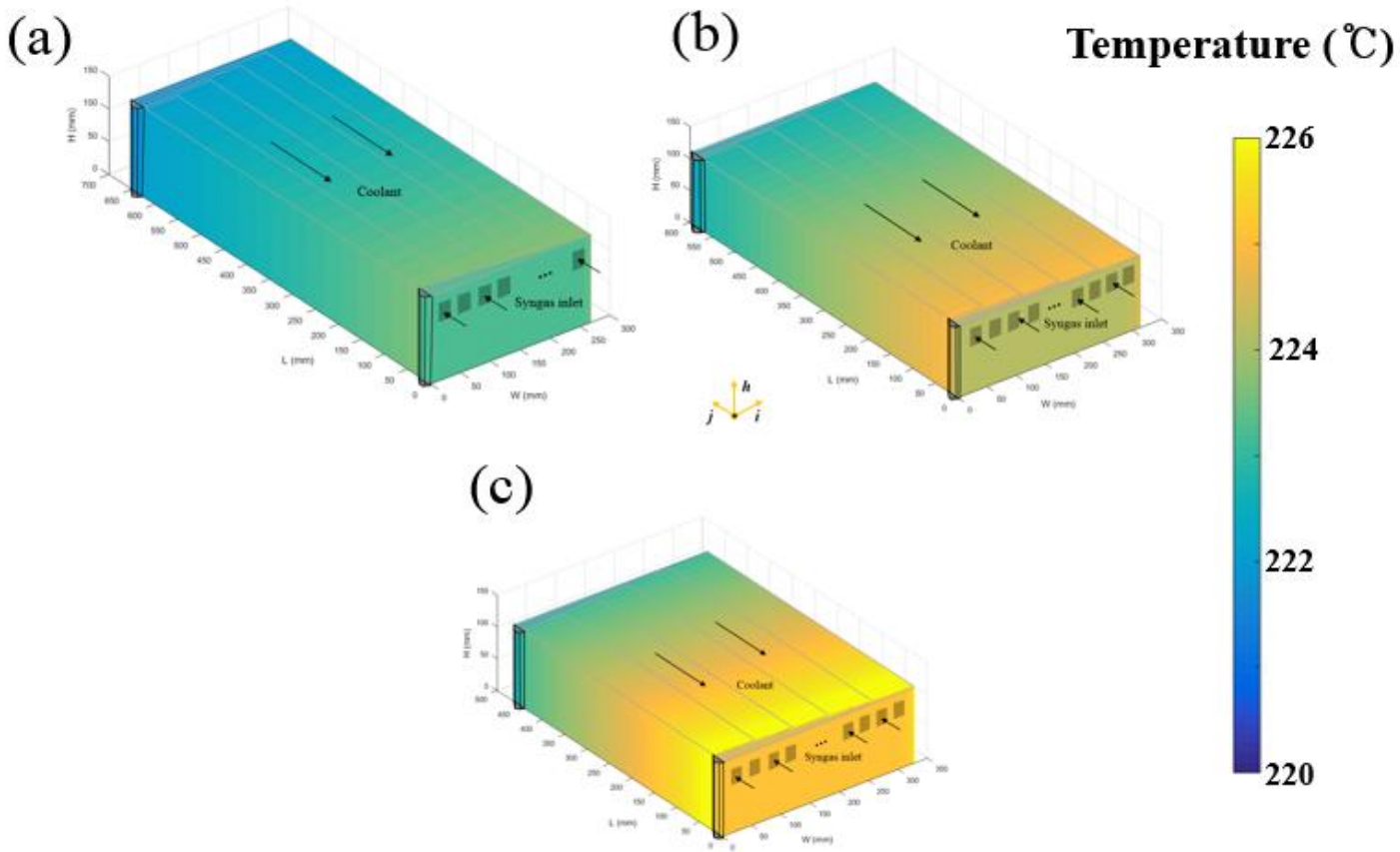

Figure 3-10. Temperature distributions of base case optimized reactor of (a) ε = 3.8 K, (b) ε = 5 K, and (c) ε = 6.2 K

Table 3-8. Representative optimization results

ε	PCH	CCH	CCW	P_{Div}	P_{Num}	MR	$n_{j,core}$	Reactor Core Volume	ΔT_{max}	n_i	n_h	Total length	Total width	Total height	ΔT_p
3.8	4.52	1	1.88	4	24	2	291	0.0459	3.77	96	14	0.653	0.268	0.134	2.03
4.4	5.04	1	1.99	5	24	2	247	0.0409	4.39	120	10	0.599	0.329	0.108	2.39
5	6.43	1	3	3	25	5	168	0.0373	4.98	75	9	0.594	0.314	0.112	2.63
5.6	7.21	1	3	3	25	5	146	0.0352	5.58	75	9	0.528	0.314	0.119	2.97
6.2	7.40	1	2.25	5	21	3	164	0.0333	6.12	105	9	0.461	0.328	0.121	3.44
6.8	7.79	1	2.56	5	18	3	137	0.0317	6.78	149	9	0.441	0.323	0.124	4.00

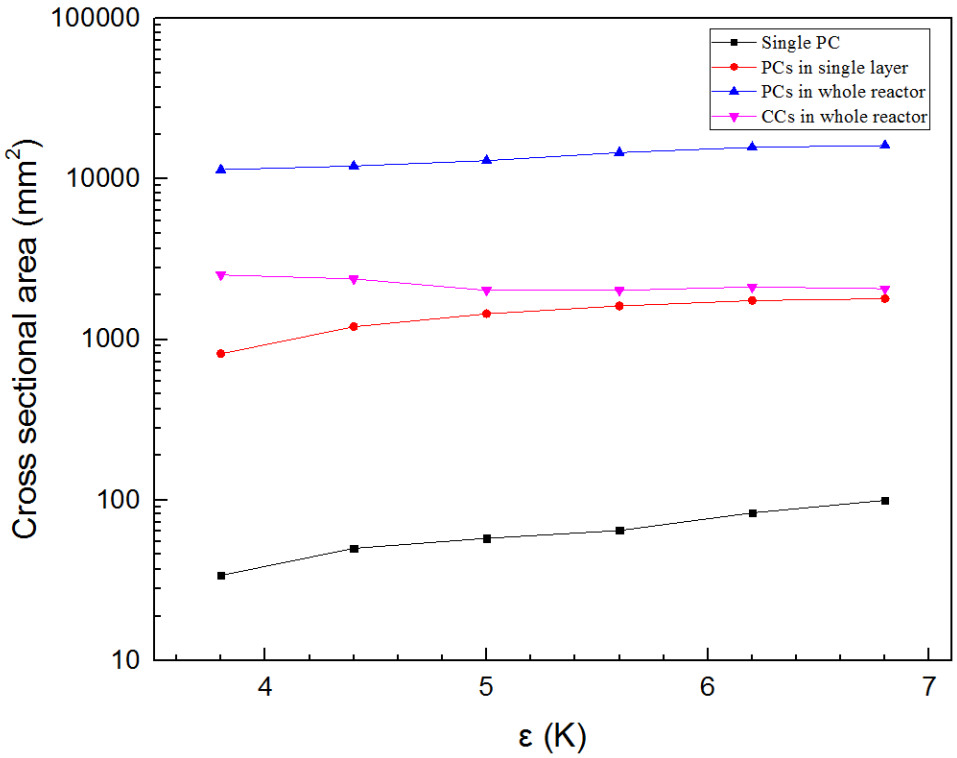

Figure 3-11. Cross sectional area of process and cooling channels

3.3.2. Coolant flowrate variation

Corresponding Pareto optimal curves of coolant flowrate variation cases generated in Table 3-4 is plotted in Figure 3-12. It is also based on following isothermal criteria.

Considering 750, 1000, and 1500 LPM, the best was not the optimal of 1500 but that of 750 and 1000 LPM at the extreme point of ε = 6.8 K. It leads from the advantage on reaction from thermal acceleration. In the 1500 LPM result of ε over 6 K, the only optimal of ε = 6 K can be obtained because high thermal performance of coolant. If we make a decision with $\Delta T_{max} > 4$ K, 1500 and 1000 LPM are rejected because former is too large for this operation condition and latter is not much difference from 750 LPM. As a result, Cases over 750 LPM shows similar performances in compared with higher flowrates. Meanwhile, case of 300 LPM should be avoided since it is too inefficient in whole range of ΔT_{max}. The difference between optimal reactor volume of 300 and 500 LPM with fixed ΔT_{max} is much larger than that of 500 and 750 LPM. We can conclude that flowrate below 500 LPM for optimal design delivers the thermal inefficiency. In this case, 500 LPM is reasonable.

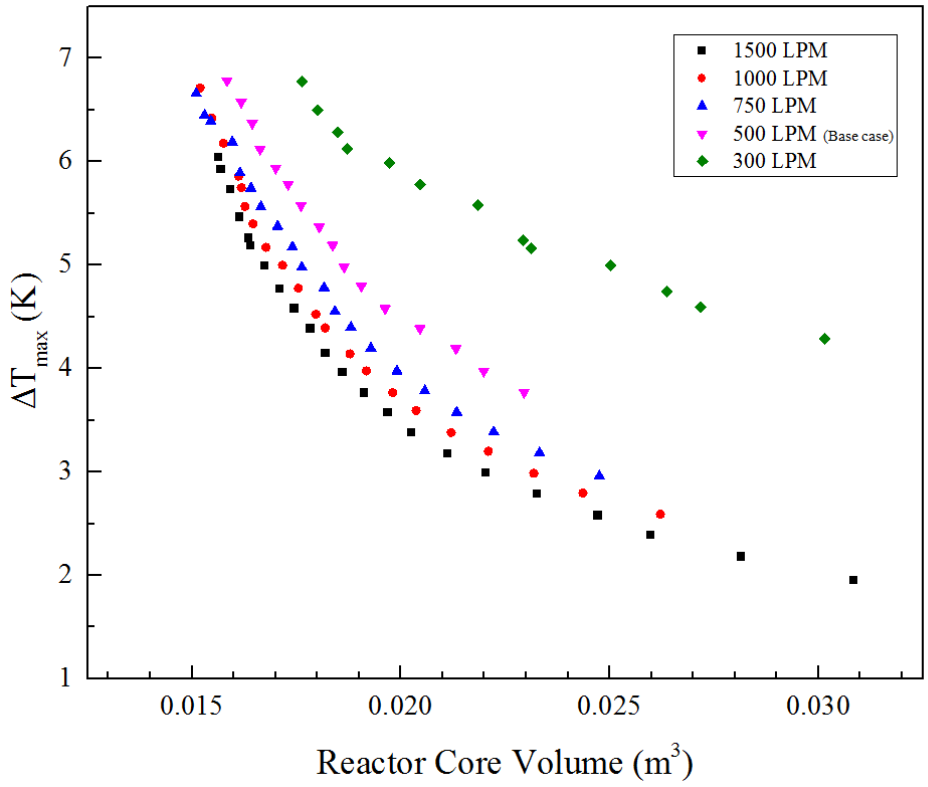

Figure 3-12. Pareto curves of various coolant rate

3.3.3. Fixed Design Parameter Effect

From Table 3-6, Pareto optimal curves obtained from ε region of 3.8~6.8 K with the interval of 0.2 K are illustrated in Figure 3-13.

The extreme cases are case 1 and 6. Their gap of optimal reactor core volume definitely leads from the features of consistently 2 times difference of all parameters with constant GSI. The apparent shapes of the rests of Pareto curves look similar but a little different depending on the regime of ΔT_{max}. Especially in ΔT_{max} over 6 K, case 2, 3, and 7 present almost same values while there is clear difference below 4 K. Meanwhile, case 4 and 5 show reverse results. That is, it is dependent of combination of parameters. Therefore, the sole influence of each parameter should be estimated from analysis of variance the with all the **ε** classes.

Table 3-9. p-values for fixed design parameters

ε	GBW	GSI	OST	PT
3.8	6.17E-04	1.40E-02	1.81E-04	9.12E-04
4	**2.37E-03**	**9.01E-02**	**6.77E-04**	**2.67E-03**
4.2	7.48E-05	3.40E-03	2.81E-05	1.01E-04
4.4	4.63E-04	1.21E-02	1.95E-04	8.07E-04
4.6	8.59E-05	1.18E-03	4.02E-05	2.02E-04
4.8	6.38E-04	7.46E-03	2.72E-04	1.50E-03
5	3.88E-04	4.18E-03	1.57E-04	7.73E-04
5.2	1.41E-04	2.02E-03	7.53E-05	3.84E-04
5.4	2.22E-04	2.87E-03	1.30E-04	6.39E-04
5.6	1.47E-04	1.46E-03	8.58E-05	4.63E-04
5.8	1.10E-04	1.09E-03	7.03E-05	3.92E-04
6	1.04E-04	1.10E-03	5.90E-05	3.35E-04
6.2	2.77E-04	2.49E-03	1.39E-04	7.81E-04
6.4	7.34E-05	7.01E-04	5.01E-05	3.03E-04
6.6	4.49E-05	3.78E-04	2.87E-05	1.91E-04
6.8	1.25E-04	1.15E-03	9.62E-05	7.73E-04

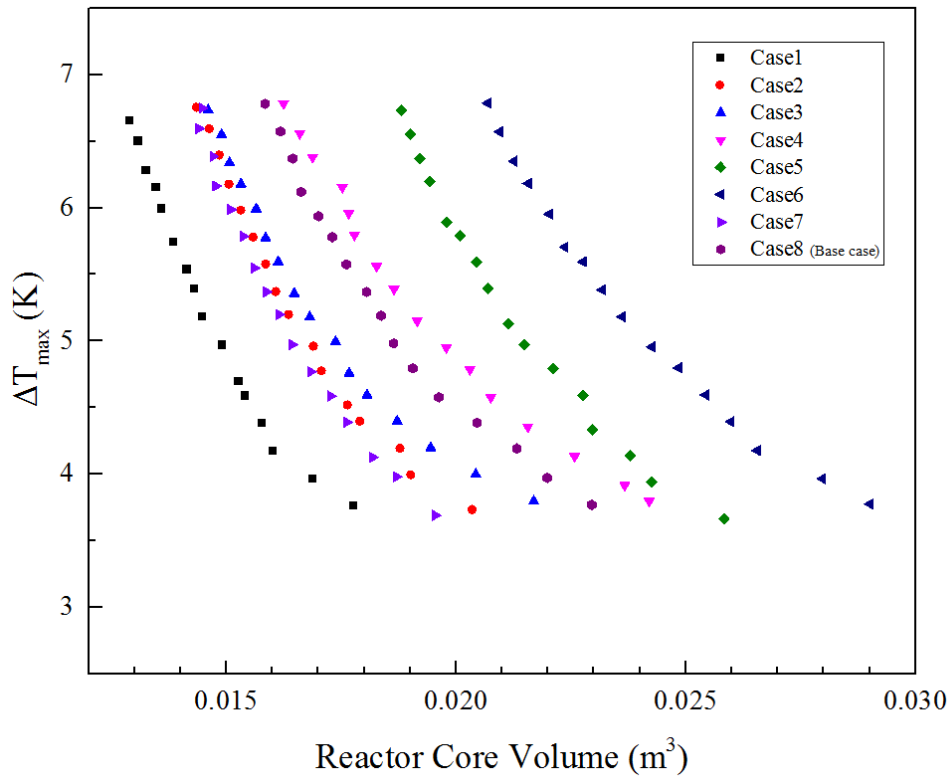

Figure 3-13. Pareto curves of various fixed design parameter

As a null hypothesis, H_0, no effect to results is defined. Its acceptance or rejection is determined by the p-value evaluated from the analysis of variance, which means the possibility of acceptance of H_0. Table 3-6 shows the estimated p-value of each ε class and parameter. The results of GSI present relatively higher than that of other parameters, and around 0.1 particularly on ε = 4 K. It seems little GSI effect on the results. The others exhibit under 10E-3 that indicates sufficient rejection of H_0. Then, independently main effect of each parameters on the optimal result should be evaluated. It is calculated like below.

$$ME_{\varepsilon,\alpha} = \frac{\sum_{y_{v,\alpha} \in L2} f_{y_v z}(x_\varepsilon^*) - \sum_{y_{v,\alpha} \in L1} f_{y_v z}(x_\varepsilon^*)}{4} \qquad (17)$$

where α is index of fixed design parameters and v is index of cases.

Figure 3-14 shows the plot of main effects on the optimal reactor volume depending on feasible ε region. It clearly presented as OST > GBW > PT all over the region. Meanwhile the magnitude of each main effect depends on the ε region. OST is definitely considered in first priority near ε = 4 K. It is 1.6 times larger than the others. In second priority, we can choose either of GBW and PT or both. Meanwhile, near ε = 6 K, OST and GBW are selectively considered as the same priority. Both of them are 1.7 times larger than PT. The consideration priority proposed above is recommended in the rest of ε region. In the different points of view, OST and PT are gradually decreased with increasing ε, but PT keeps constant. User can consider any combination with the recommended priority.

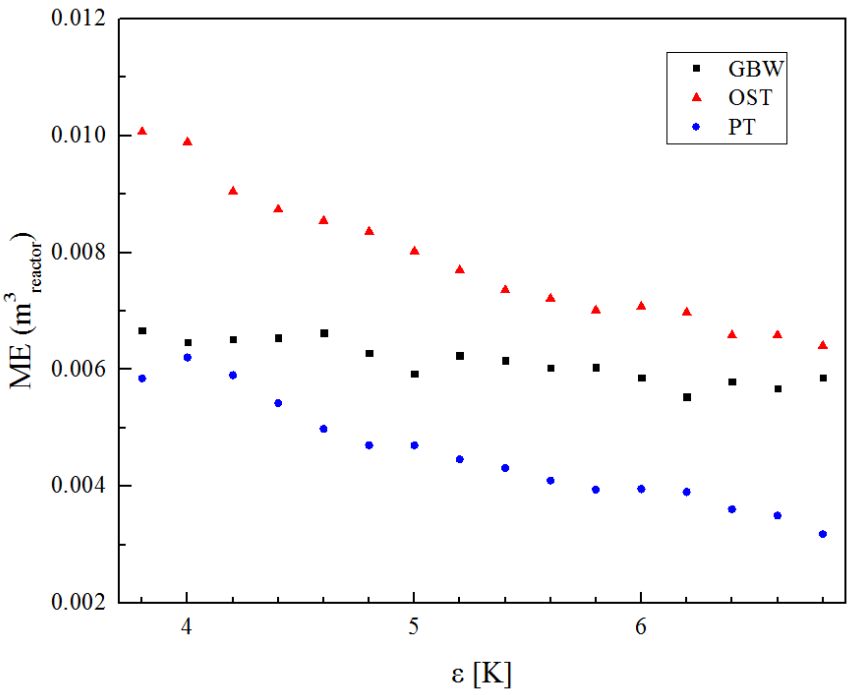

Figure 3-14. Main effect of 3 fixed design parameters

3.4. **Conclusions**

Microchannel FTS reactor model was constructed using cell coupling method and optimized with the objectives such as reactor core volume and ΔT_{max}. Those represent compactness and operation safety. The Pareto optimal set can be obtained from the surrogate model optimization. Users can select the optimal design from their design condition with interest. Optimized design in the multi-channel scale phase is highly remarkable for considering entire heat and mass transfer performance for entire reactor. It is useful and economical to set the design guide in conceptual reactor design. Through the additional analysis process conducted in this article, optimized reactor with reasonable cooling medium flowrate and fixed design parameters can be determined as well. In Pareto optimal study of 0.5 C_{5+} microchannel reactor design, 500 LPM was selected as the reasonable flowrate and the consideration priority was Outer shell thickness > Guide bar width > Plate thickness when the modification was required from the original optimal condition. Further mechanical stress calculation is necessary for detailed design phase. It can be discussed with fabrication company. From this analysis process, more efficient decision making in industry will be possible in the conceptual optimal reactor design set of exothermal and even endothermal microchannel type reactor with whole operation conditions and configuration.

CHAPTER 4: Optimal design of Fischer-Tropsch synthesis system using genetic algorithm

4.1. Background

Low temperature (LT) FTS process is well known as the promising route to produce eco-friendly liquid fuel with high efficiency connected with synthesis gas conversion process[45]. The cobalt type catalyst is used in that water gas shift (WGS) and C1 formation reactions are lower level than high temperature FTS. Due to inherently highly exothermic feature, the reactor is required to have capability to remove reaction heat effectively for stable operation. Among the types of high performance reactors, microchannel reactor is popular in the liquid fuel production of small to middle capacity. It shows the manner of layer stacked for ease of scale-up.

In particular, the gas conversion process for producing Syngas, which is the raw material of FTS, is a very capital-intensive process, so FTS process with high carbon and economical efficiency is essential for efficient fuel liquid synthesis process. The ultimate goal of increasing carbon efficiency is to increase the efficiency of the process because if the incoming carbon source is not converted to the desired liquid fuel, it is converted to CO2 as final sink after combustion inside the process.

A multi-stage FT process study was proposed as one of the studies to improve the carbon efficiency. Dai et al. conducted the experiments of the single-stage

performance of a 12-m fixed bed FT reactor and multi-stage with two 6-m reactors that water vapor removed after the first reactor. They concluded multi-stage showed more than 10% in diesel production and an increase in carbon efficiency of 0.77[46]. According to literature, generally carbon efficiency shows 25-50% in biomass to liquid process with single staged. In gas to liquid, carbon efficiency increases up to around 0.67 with multi-staged and up to around 0.62 with single staged[47]. The objective of multi-staged FTS is to increase the reactivity by eliminating the water vapor in the middle of the reaction, because the partial pressure of the product water vapor increases as CO conversion increases. Also, when the partial pressure of water vapor increases, the sintering of the catalyst accelerates and causes irreversible deactivation[48, 49]. However, when the multi stage FT reaction system is applied, there is a disadvantage in terms of capital cost rather than the existing single stage because the reactor is split into two and the cooler and additional separator are installed to remove the water vapor. There has been no quantitative analysis of the existing single stage and economical aspects, and this analysis is essential to assure sustainability of FTS stand-alone process.

In this study, we construct the superstructure process which can consider single stage, multi stage FTS, recycle, and WGS reaction in the stand alone FTS system using microchannel reactor, and we obtained economically most advantageous FTS structure. Genetic Algorithm was used for optimization.

4.2. **Problem description**

Figure 4-1 shows the schematic diagram of the FTS system superstructure to be analyzed in this study. The overall process incorporates the following three structures: 1) Section A: Single stage of FTS without recycle

2) Section A+B: Single stage of FTS with recycle

3) Section A+C: Double stage of FTS

This main processes are determined by two splitter, SP1 and SP2. Both SP3 and SP4 adjust a H_2/CO ratio of syngas entering the next FTS reactor. The H_2/CO ratio becomes lower than the inlet at the outlet of FT reactor. The syngas with lowered ratio results in less reactive. In the entire GTL process including the syngas production process, the tail gas is recycled to the reforming process and syngas with a high H2 / CO ratio is reproduced. In other words, although WGS reactors are not considered in general, those can be considered as an option as an economical syngas ratio control device due to the characteristic of FTS stand-alone system. The target product is C_{5+} 1000 BPD and is obtained from streams 9 and 10 in Figure 4-1. Syngas feeds are adjusted to process conditions. The FTS reactor core was delivered based on the microchannel technology following the reactor structure disclosed by Velocys Inc., a leading company in microchannel reactor field[50].

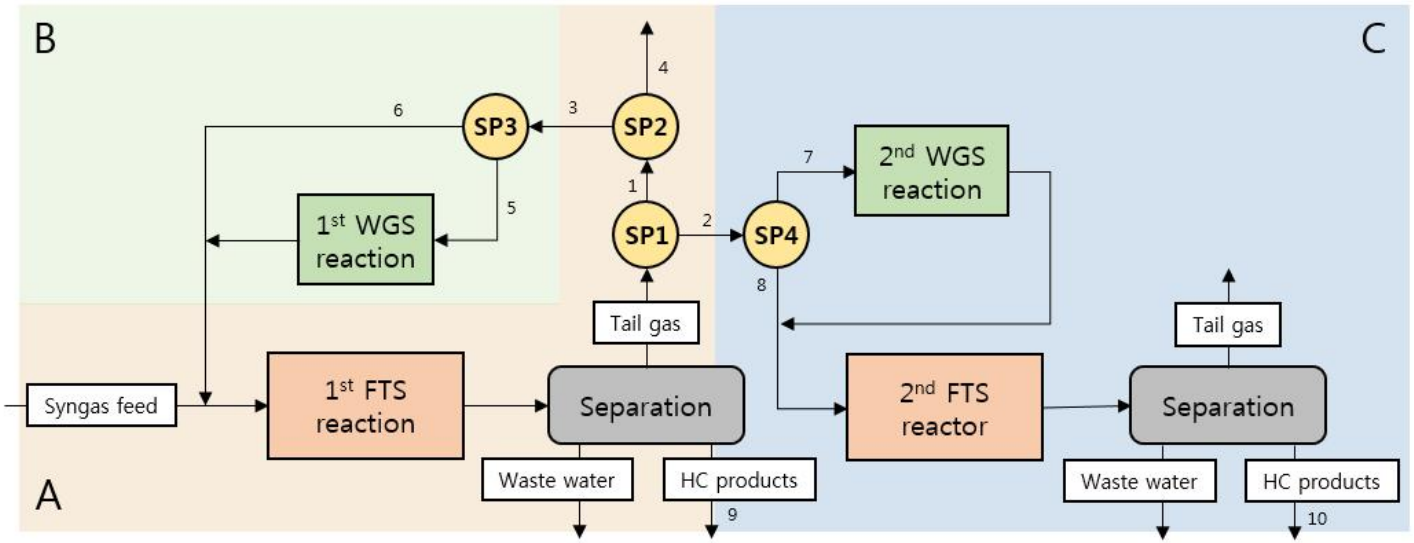

Figure 4-1. Schematic block diagram of superstructure FTS system

The ultimate goal is to find the most economical structure in this process at higher conditions than the single stage carbon efficiency published in the previous literature. The total number of optimization variables is 12 such as the split ratio of each splitter (4), the reactant inlet temperature (4) to each FTS and WGS reactor, the number of channels of the microchannel FTS reactor (2), and the flow rate of the reactant (2). The optimization was performed using MATLAB® 2016B and the economics model was modeled using MATALB code and ASPEN® Plus linked.

4.2.1. Model description

Figure 4-2 shows a detailed superstructure of the schematic block diagram using ASPEN PLUS, commercial process modeling program. The determinants of the individual processes incorporated in the superstructure are the SP-01, SP-02, SP-03, and SP-04 splitter units. SP-01 represents the flow fraction to SINGRXT stream over total flow and is a binary integer that selects whether to select single stage (value = 1) or multistage (0). SP-02 determines the recycle rate of the flow fraction to RECY-INL stream. It has a value of 0 ~ 1. In order to compensate for the decrease of the H2 / CO ratio of the syngas through the FT reaction, the addition of hydrogen source through the WGS reaction is partially required for recycle stream flowing into the main stream. The SP-04 also plays the same role as the SP-03, in order to control the reduced H2 / CO ratio when applied to the multi-stage. Table 4-1 summarizes 12 optimization variables.

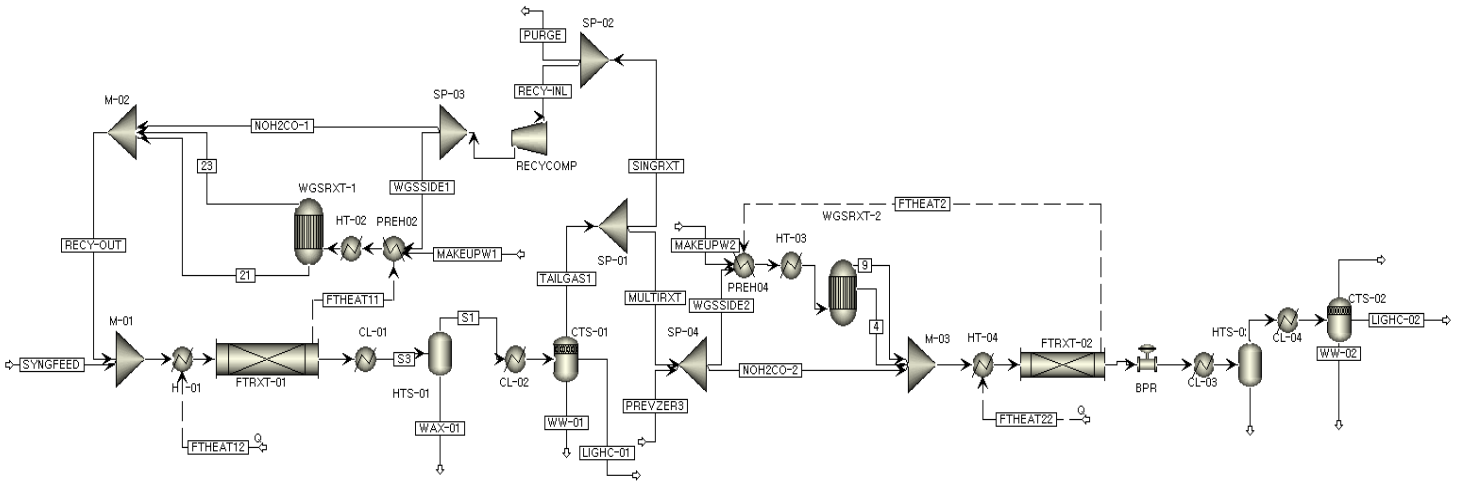

Figure 4-2. Detailed Superstructure of Fischer-Tropsch synthesis standalone process built by ASPEN® Plus v. 8.8

Table 4-1. Optimization variables

ID	Variables	LB_i	UB_i	Unit	Description
1	NoLFT1	20	20000	-	Number of layers for FTS1 reactor
2	NoLFT2	2	2000	-	Number of layers for FTS2 reactor
3	SR1	0	1	- (Binary variable)	Split ratio to single stage (with multi stage)
4	SR2	0	1	-	Split ratio to recycle stream (with purge)
5	SR3	0	1	-	Split ratio to WGS1 stream (with no H2/CO ratio change stream)
6	SR4	0	1	-	Split ratio to WGS2 stream (with no H2/CO ratio change stream)
7	TinFT1	200	220	℃	Inlet temperature of FT reactor-1
8	TinFT2	200	220	℃	Inlet temperature of FT reactor-2

9	TinWGS1	200	250	℃	Inlet temperature of WGS reactor-01
10	TinWGS2	200	250	℃	Inlet temperature of WGS reactor-02
11	MW1	0	0.05	kmol/s	make up water for WGS1 reaction
12	MW2	0	0.05	kmol/s	make up water for WGS2 reaction

Detailed dimension of single channel (width, height, and length) is fixed, and 400 pieces are gathered to be single layer. Since the number of layers is directly related to the reactor capital cost, it should be included in the decision variable of this superstructure as a design consideration.

The pressure of the separators affect the separation performance, which leads to a composition change in the tail gas stream, but is not included in the optimization parameter. Since the pressure at the front end of the reactor is fixed and the single channel dimension of the reactor is also determined, the outlet pressure of reactor can be determined constantly. In the case of this dimension reactor, the pressure of the HT separator is fixed because a ΔP of about 3 bar is determined even if the number of layers becomes varied. However, the ΔP of the separator can be changed according to the detailed design, but in this study, the design margin is fixed by fixing the ΔP to 0.5 bar, the pressure is fixed in the conceptual design stage and the simple separators are used. The target product to be studied in this study is a stand-alone process of C5 + 1000 BPD class and uses a microchannel-type reactor, which is very strong in small- to middle-scale FT systems[51]. To quantitatively derive the ultimate goal of carbon efficiency in this study, we use the product kinetics published by Velocys[50]. They are presented in Table 4-2 below.

Table 4-2. Reaction rates and kinetic parameters for Fischer-Tropsch catalyst in literature

ID	Reaction equation	Reaction rates [Concentrations in kmol/m^3]	k_i [rates in kmol /(kg_{cat} s)]	E_i [$\frac{J}{kmol}$]
1	$3H_2 + CO \rightarrow H_2O + CH_4$	$r_{CH_4} = k_1 exp(-E_1/RT) C_{H_2}$	2.509×10^9	1.30×10^8
2	$5H_2 + 2CO \rightarrow 2H_2O + C_2H_6$	$r_{C_2H_6} = k_2 exp(-E_2/RT) C_{H_2}$	3.469×10^7	1.25×10^8
3	$7H_2 + 3CO \rightarrow 3H_2O + C_3H_8$	$r_{C_3H_8} = k_3 exp(-E_3/RT) C_{H_2}$	1.480×10^7	1.20×10^8
4	$9H_2 + 4CO \rightarrow 4H_2O + C_4H_{10}$	$r_{C_4H_{10}} = k_4 exp(-E_4/RT) C_{H_2}$	1.264×10^7	1.20×10^8
5	$H_2O + CO \rightarrow H_2 + CO_2$	$r_{CO_2} = k_5 exp(-E_1/RT) C_{H_2}$	2.470×10^7	1.20×10^8
6	$29H_2 + 14CO \rightarrow 14H_2O + C_{14}H_{30}$	$r_{C_{14}H_{30}} = \frac{k_6 exp(-E_6/RT) C_{H_2} C_{CO}}{[1 + k_{ad} \exp\left(-\frac{E_{ad}}{RT}\right) C_{CO}]^2}$	3.165×10^4 $k_{ad} = 63.5$	8.0×10^7 $E_{ad} = 8.0 \times 10^7$

Catalyst diameter is 250 μm and bed density is 1060 kg / cum. In the FT reactor, the dimensions of a single channel are fixed with a width of 0.04″, a height of 0.225″, and a length of 23″, which is the commercial dimension scale of Velocys[50]. The reactor is designed as a channel numbering up and assumes that the reaction temperature is maintained under isothermal condition due to the introduction of sufficient coolant. The pressure is 25 barg and the temperature is 25 ℃.

The H_2 / CO ratio of the feed syngas is fixed at 2 and the flowrate is varied to match the target product 1000 bpd. Nitrogen is introduced into feed syngas with molar composition of 0.04. The feed gas is mixed with the recycled syngas and heated to the reaction temperature via the heater HT-01. After the reaction, the product is cooled to 130 ° C to separate WAX-01 in HTS-01. The remaining vapor is cooled to 30 ° C and separated into waste water, light hydrocarbons, and tail gas in a three-phase separator CTS-01.

In the single FT stage, the tail gas flows to the SINGRXT stream through SP-01. In the SP-02 splitter, a part of it flows out to the PURGE stream and the pressure of recycle stream is compensated by the recycle blower. Because there is little water in the stream, enough make up water is supplied from waste water. Through the preheater PREH02 and the fired heater HT-02, it goes up to the temperature range of the LTWGS reaction and flows into WGSRXT-1. The WGS reaction here is a low temperature WGS operated mainly in the region of 200-250 ° C and can reach the equilibrium rapidly in about 0.09 seconds, mainly using Cu series catalysts[52].

$$CO + H_2O \leftrightarrow CO_2 + H_2 \qquad \Delta H^0{}_{298\,K} = -41.09 \frac{kJ}{mol} \qquad (4-1)$$

In the case of Multi stage, the H2 / CO ratio is controlled by SP-04 splitter in the same role as SP-03. The temperature of the reactant flowing into the second FT reactor is increased by HT-04. The product is lowered to atmospheric pressure by a back pressure regulator (BPR unit), which also separates the wax and light hydrocarbons in HTS-02 and CTS-02.

4.2.2. Reactor model validation

The FT reaction temperature range is 200 ~ 220 ℃, and the graph of comparison between the reactor model estimated and experimental data is shown in Figure 4-3 and Table 4-3[50, 53, 54]. We can adopt the reactor model with sufficient validity.

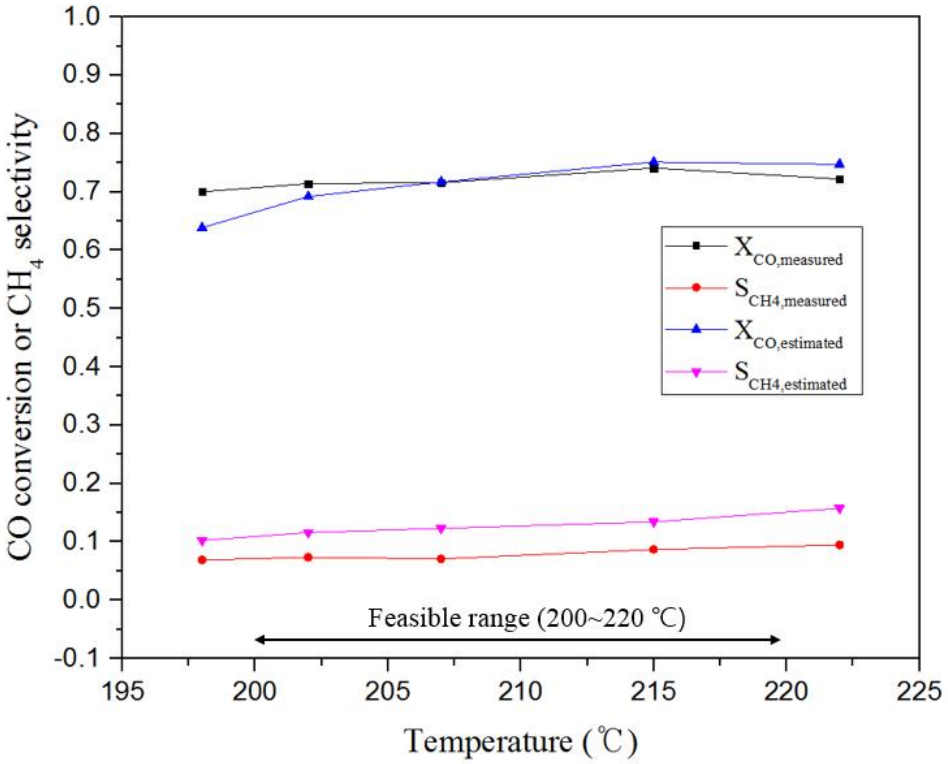

Figure 4-3. Model estimation and experimental literature data of CO conversion and CH4 selectivity

Table 4-3. Model validation set specification

ID	GHSV(hr^{-1})	H_2/CO ratio	Inert(N_2) composition	Temperature(℃)	$X_{CO,measured}$	$X_{CO,estimated}$	$S_{CH4,measured}$	$S_{CH4,estimated}$
1	12413.8	2.03	0.168	198	0.700	0.639	0.069	0.102
2	12413.8	2.03	0.168	202	0.714	0.692	0.074	0.116
3	12413.8	2.03	0.168	204	0.716	0.717	0.071	0.123
4	12413.8	2.03	0.168	207	0.741	0.751	0.087	0.134
5	17142.9	2.00	0.167	215	0.722	0.747	0.095	0.158
6	24000.0	2.01	0.166	222	0.710	0.737	0.143	0.181

4.2.3. Economic cost model

The conceptual economics cost model used refers to the cost based model proposed in the literature[55, 56]. The CE index is calculated as 580 based on 2015. The purchase cost correlation of each equipment to obtain the inside battery limit (ISBL) cost is as follows.

For the microchannel reactor, use the inhouse cost model. Empirically, the reactor takes the form of a cost per unit layer. Four hundred channels constitute a single process layer and a unit layer is formed with the process layer abutted. Material cost per layer is about $ 350 based on 2015. Reactor purchase cost can be obtained as follows.

$$\mathrm{C}_{B,\mathrm{FTR}}\,(\$) = 350 \cdot total\ number\ of\ unit\ layers \qquad (4-2)$$

$$\mathrm{C}_{P,\mathrm{FTR}}\,(\$) = F_{aux} \cdot F_{mfg} \cdot \mathrm{C}_{B,\mathrm{FTR}} \qquad (4-3)$$

where F_{aux} represents the factor of auxiliary cost for braket, external distributor, and sealing equipment, and F_{mfg} indicates the factor of manufacturing process. Let F_{aux} and F_{mfg} be 1.5 and 2.7.

The pressure vessel is applied to the HTS-01, HTS-02, CTS-01, CTS-02, WGSRXT-1 and WGSRXT-2 units.

$$\mathrm{C}_{P,\mathrm{Vessel}}\,(\$) = \mathrm{F}_M \mathrm{C}_V + C_{PL} \qquad (4-4)$$

$$\mathrm{C}_\mathrm{V} = \exp(6.775 + 0.18255 \cdot ln(W) + 0.02297 \cdot ln(W)^2) \qquad (4-5)$$

where $\mathrm{F_M}$ is material factor that is assumed as 1 with carbon steel and W represents vessel weight in lb. $\mathrm{C_{PL}}$ is the cost for platforms and ladders, which

depends on the vessel layout:

$$C_{PL} = 285.1 \cdot (D_i)^{0.7396} \cdot (L)^{0.70684} \quad (4-6)$$

where D_i (inner diameter) and L (length) are in ft. In general, L / D ratio = 3 is used as the rule of thumb in the pressure vessel. The liquid hold up time of this pressure vessel is τ_{hold} = 5 min and τ_{surge} = 2 min. Assuming H_{LLL} follows $\tau_{LLL} = 1 / 2\tau_{surge}$, the vessel length can be calculated as follows.

$$L = 2(H_{LLL} + H_S + H_H) = 3H_S + 2H_H \quad (4-7)$$

For the fired heaters(HT-02, HT-03),

$$C_{P,Fired\ Heater}\ (\$) = F_P F_M C_B \quad (4-8)$$

where C_B, the base cost, is a function of the heat duty.

$$C_B = \exp(0.8505 + 0.766 \cdot \ln(Q)) \quad (4-9)$$

where Q is in Btu/hr. F_P and F_M are for the pressure and material effect, and both were assumed to be 1 in this study.

For the heat exchangers (HT-01, CL-01, CL-02, PREH02, PREH04, HT-04, CL-03,and CL-04 in Figure 4-2), The shell and tube type heat exchanger were adopted as expressed below.

$$C_{P,HEX}\ (\$) = F_P F_M F_L C_B \quad (4-10)$$

$$C_B = \exp\{11.0545 - 0.9228[ln(A)] + 0.09861[ln(A)]^2\} \quad (4-11)$$

Where F_P is pressure factor with 1.05 for around 25 bar and F_M is material factor set as 1 with carbon steel and F_L is tube length correction factor set as 1 with 20 ft under assumption.

The turbo blower is used as a recycle compressor. The purchase cost can be estimated as follows.

$$C_P = F_M C_B \qquad (4-12)$$

$$C_B = \exp(6.6547 + 0.7900[\ln(P_C)]) \qquad (4-13)$$

where P_C is net power in horse power, F_M is material factor with cast aluminum blade of 0.6. This blower is driven by motor. The motor efficiency is 0.92.

The f.o.b. onsite cost can be obtained by applying Hand's factors listed in Table 4-4 including delivery, installation, instrumentation, and test-run cost for each equipment. All capital cost correlations except for microchannels are adjusted to mid-2000 (CE index = 394), so it is necessary to revise the current price as 2015.

Fixed capital investment (FCI) and total investment cost (TIC) can be evaluated using the following correlation equation.

$$\mathrm{FCI} = 1.25 \cdot 1.45 \cdot (\mathrm{Onsite}) = 1.8125 \cdot (\mathrm{Onsite}) \qquad (4-14)$$

$$\mathrm{TIC} = 1.3 \cdot \mathrm{FCI} \qquad (4-15)$$

Table 4-4. Hand's factors summary

Hand's factor (i)	Reactor	Compressor	Heat exchanger	Pump	Vessel
H_i	4.6	2.8	4	4.6	4.6

For estimation of operating cost, 10% of constant depreciation allowance and 30% income tax was assumed. Total product cost (TPC) follows the below correlation.

$$\begin{aligned}\text{TPC} &= \text{Manufacturing cost} + \text{SARE} \\ &= (\text{Direct production cost} + \text{Fixed charge} + \text{Plant Overhead}) \\ &\quad +0.025(Revenue) \\ &= 1.03(\text{Raw material} + \text{Utility}) + \text{Labor} + 0.186(\text{Onsite}) \\ &\quad +0.025(Revenue) \qquad (4-16)\end{aligned}$$

$$\text{Profit before tax} = \text{Revenue} - \text{TPC} \qquad (4-17)$$

$$\text{Profit after tax} = (1-0.3)(\text{Profit before taxes} - \text{Depreciation}) \qquad (4-18)$$

where SARE represents sales, administration, research, and engineering.

Payout time can be considered representative profitability index as follows:

$$\text{Payout time (yr)} = \frac{FCI + Start\ up\ cost}{Profit\ after\ taxes + Depreciation} \qquad (4-19)$$

where Start up cost indicates the cost for test run and start-up for the plant. It costs about 10% of FCI. The syngas production cost and wax sales cost were assumed as 40 $ per thousand cubic meter and 1000$/ton[57].

As shown in Figure 4-4, an integrated model was established to link the MATLAB and ASPEN Plus models to evaluate profitability and carbon efficiency.

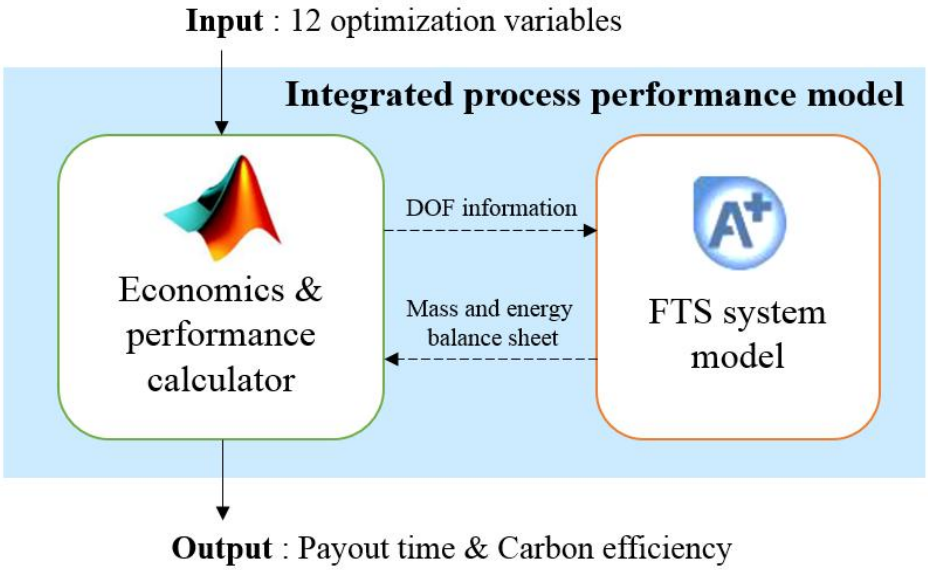

Figure 4-4. Structure of process performance model

4.2.4. Optimization methodology

Because of the nature of the problem, we need to analyze the economics model using a highly nonlinear process model, so we adopted the genetic algorithm as the global search algorithm which is the most widely used among the derivative-free optimization algorithms. A brief formulation of the optimization problem is as follows.

$$\text{Minimize Payout time}$$

$$\text{s.t.}$$

$$\text{Carbon efficiency} > 0.6241$$

$$\mathrm{LB}_i \leq x \leq \mathrm{UB}_i \qquad where\ i = 1..12 \qquad (4-20)$$

The specific carbon efficiency constraint is set from the value obtained from the carbon efficiency maximization study dealing with a single stage FTS reactor in pervious literature[47]. The only FTS system derived with satisfaction of constraint has an advantage. LBi and UBi indicate lower and upper bound of optimization variables listed in Table 4-1. The GA algorithm can be implemented using Matlab. Optimization is performed by changing various options to improve reproducibility and reliability. The population size and crossover fraction were changed. The population size set was composed of 200, 300, ..., 1000, and the crossover fraction set were 0.5, 0.8. A total of 18 optimizations were repeated for the same problem. The best solution among the optimal candidates was selected. The flow chart of optimization shows below in Figure 4-5.

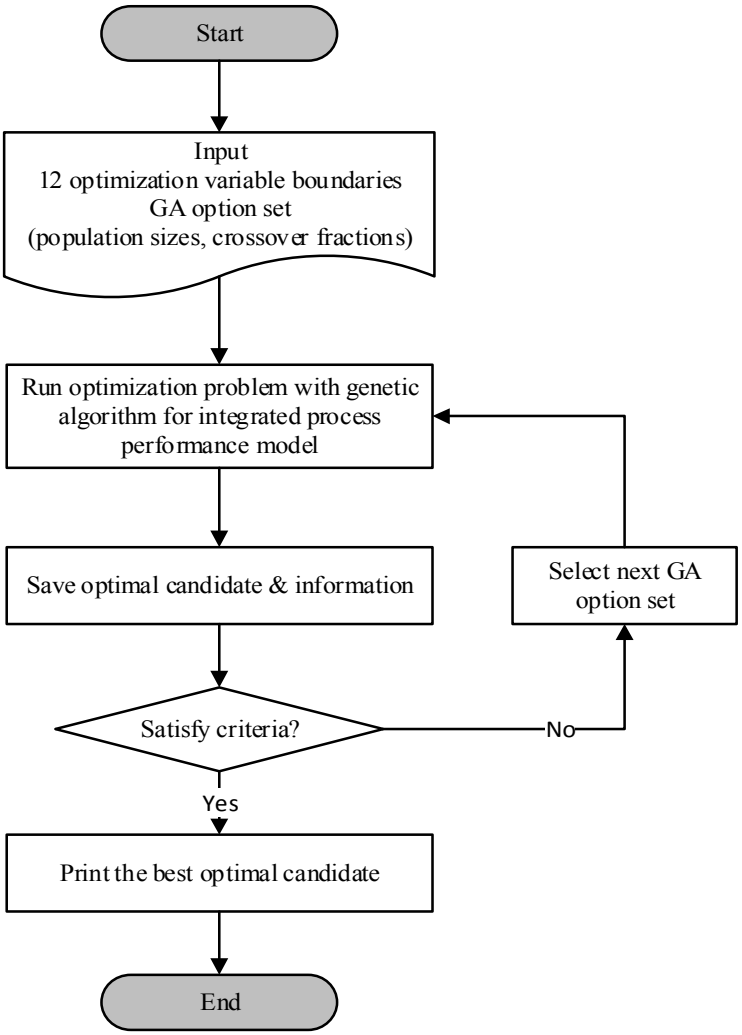

Figure 4-5. Schematic flow chart of optimization

4.3. **Result and discussion**

In this section, optimization of the superstructure was performed using 12 variable as the optimization variable. As a result, FTS standalone optimal process was derived. The results are shown in the first column of Table 4-5. Single stage with recycle was evaluated as the most economical process. For the comparison with other main processes which are multi-stage process and the single staged without recycle, results are obtained by fixing the SR1 and SR2 as parameters and shown in 2nd and 3rd column of Table 4-5. Table 4-5 (a) shows the values of objective function and variables as optimization results. (B) presents the process key operating condition and (c) summarizes the economical evaluation.

Table 4-5. Optimization summary: (a) optimization result; (b) optimal process condition; (c) profit summary

(a)

Variables	Optimal of superstructure	Optimal of multi-stage	Optimal of single stage w/o recycle	Units
NoLFT1	2293	1575	2717	-
NoLFT2	-	1533	-	-
SR1	1	0 (fixed)	1 (fixed)	-
SR2	0.6948	-	0 (fixed)	-
SR3	0	-	-	-
SR4	-	0	-	-
TinFT1	205.55	211.66	200.91	℃
TinFT2	-	204.23	-	℃
TinWGS1	-	-	-	℃
TinWGS2	-	-	-	℃
MW1	-	-	-	kmol/s
MW2	-	-	-	kmol/s
Optimal Payout time value	1.84	2.31	2.14	year

(b)

Operating conditions	Optimal of superstructure	Optimal of multi-stage	Optimal of single stage w/o recycle	Units
Syngas feed rate	0.48	0.43	0.50	kmol/s
CO Conversion of FTR1	0.48	0.61	0.74	-
CO Conversion of FTR2	-	0.64	-	-
C1 selectivity of FTR1	0.09	0.09	0.10	-
C1 selectivity of	-	0.12	-	-

FTR2				
Carbon efficiency	0.64	0.72	0.63	-

(c)

Economical evaluation	**Optimal of superstructure**	**Optimal of multi-stage**	**Optimal of single stage w/o recycle**	**Units**
Revenue	4.19E+07	4.19E+07	4.19E+07	$/yr
Total Product Cost	1.84E+07	1.78E+07	1.91E+07	$/yr
Profit before tax	2.35E+07	2.42E+07	2.28E+07	$
Profit after tax	1.44E+07	1.42E+07	1.36E+07	$
TCI	3.77E+07	4.94E+07	4.29E+07	$
FCI	2.90E+07	3.80E+07	3.30E+07	$
ROI	38.35	28.86	31.78	%

All three processes rejected the WGS reaction economically. This is because the capital cost of installing a WGS reactor and a heat exchanger is larger than the profit generated by increasing the reactivity by raising the lowered H2 / CO ratio. In all three cases, the reactor accounts for about 20% of the total equipment cost.

Superstructure optimal recycles about 70% of the tail gas. The CO conversion of the reactor is low because the flow into the reactor combined with the main stream is 60-80% larger than the other two optimal structures. Also, low CO conversion has the effect of not diluting the main stream syngas much because the fraction of syngas in the tail gas is high. The highest profitability occurs because the total capital investment is lowest.

In the case of the multi-stage, the syngas feed rate is the lowest because the carbon efficiency is basically higher than the other two cases, which is advantageous for the total product cost. However, the total number of channels in the two reactor is about 30% more than the superstructure optimal process, and there is another separation process, which is the most disadvantage in capital cost.

Finally, in the case of the simple FTS single stage process, the CO conversion is in the UB constraint and maximizes the product selectivity by minimizing the reaction temperature because all the incoming syngas must maximize the yield with one reactor. It is simple but has higher profitability than multi stage.

In this study, optimization was performed by setting syngas production cost at 40 $ / TCM and product sales price at 1000 $ / ton. However, the price of carbon sources such as coal and natural gas, which are raw materials of syngas, and the

product sales price may fluctuate. Sensitivity analysis was performed on these two cases.

Figure 4-6 shows the syngas production cost variation effect to profitability. The lower profitability of all processes are shown with the cost increased. That is, the payout time increases and the required time for the investment cost recovery increases. However, unlike the two processes, the profitability of the multi-stage system is higher than the single stage without recycle at about 60 $ / TCM and higher than superstructure optimal at 90 $ / TCM. This is because the multi-stage process has a high carbon efficiency and the required syngas feed rate is relatively low, so that the total production cost takes the economical advantage at the boundary point. However, since the level of 90 $ / TCM is extreme case at syngas production cost, most superstructure optimal structure is absolutely superior[57].

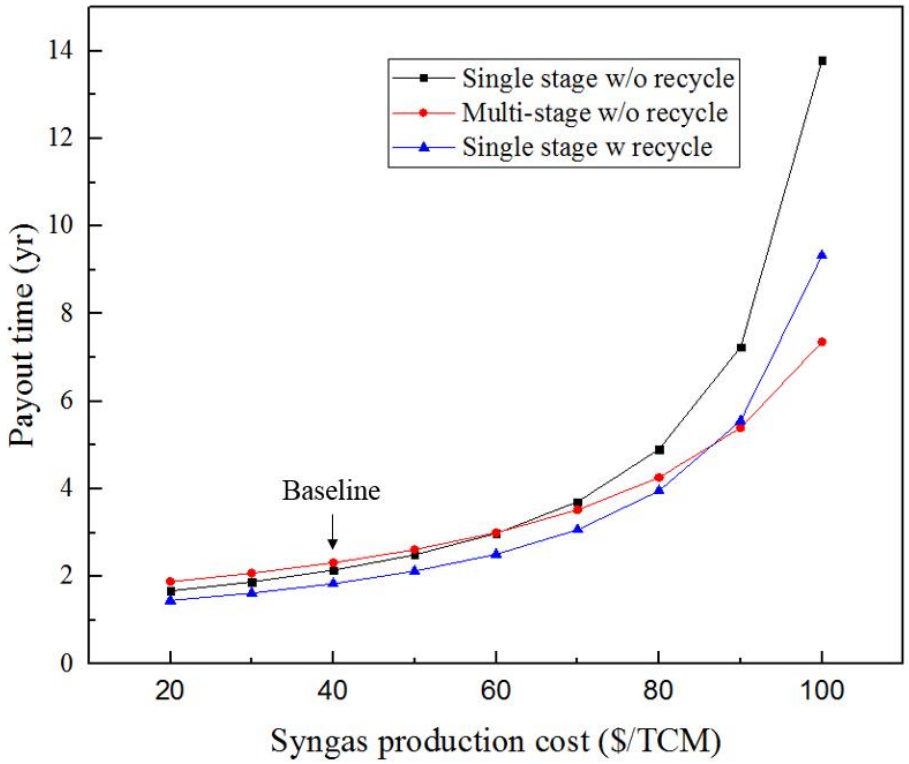

Figure 4-6. Payout time corresponding to syngas production cost variation

Figure 4-7 shows the profit after tax, which shows that multi-stage is more advantageous than other two processes over $ 50 / TCM. In terms of profit, it can have a conditional superiority than superstructure optimal. Simple Single stage is absolutely disadvantageous compared to the other two cases. Figure 4-8 presents the results of profitability with changes in product sales price. In all cases, the superstructure optimal is absolutely superior to the other two cases, and when multi-stage is reduced by more than 30% from the baseline, it dominates the simple single stage.

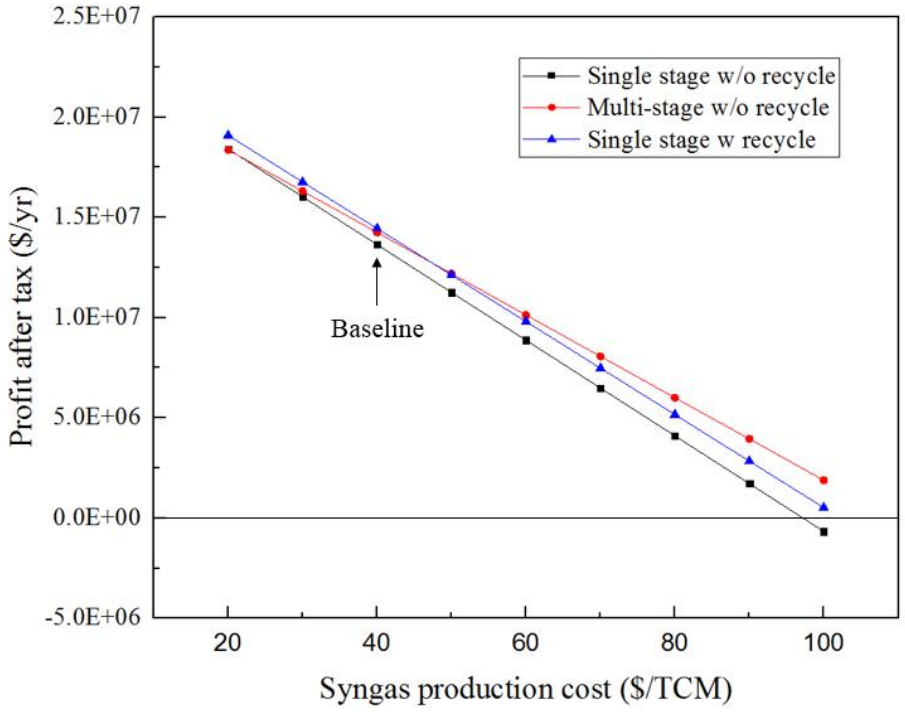

Figure 4-7. Profit corresponding to syngas production cost variation

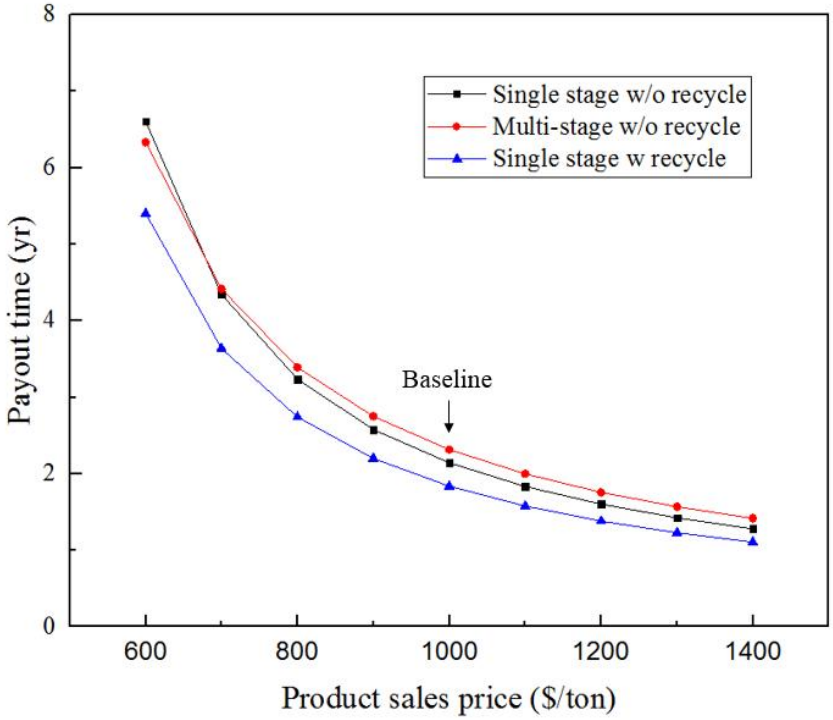

Figure 4-8. Payout time corresponding to product sales price

4.4. **Conclusions**

The superstructure of FTS stand-alone system was constructed and optimized with objective function of profitability which was payout time. It included the single stage FTS, multi-stage, recycle, and WGS reaction which were considered as the routes for process efficiency improvement. The single staged FTS with recycle was obtained as superstructure optimal. In order to compare with other main processes such as multi stage and single stage without recycle, they were also partially optimized with some of determinants fixed.

In the case of superstructure optimal, the profitability is dominant over the other two cases because the capital cost is the lowest, and the multi stage is disadvantageous since the total production cost is low but the capital cost cannot exceed it. In the syngas production cost and product sales price discussed in this study, profitability is advantageous in order of superstructure optimal> single stage without recycle> multi stage. In all three cases, consideration for the WGS reaction was rejected economically. Superstructure optimal absolutely takes the advantage of whole variation region for sales production cost and product sales price compared with other two processes.

CHAPTER 5: Concluding Remarks

5.1. Conclusions

This thesis has addressed the optimal design of sustainable Ficsher-Tropsch synthesis stand-alone utilizing microchannel type reactor. Single layer, overall reactor, and whole FTS process design have been considered and validated with experimental data in pilot scale.

At first, a simple trapezoid-shaped guiding fin was introduced to achieve a uniform distribution in microchannel layer composed of 110 main channels. The upper length was found to locally affect the main channel distribution near inlet, whereas the bottom one influenced the distribution far from the inlet. The optimal design deliver the improvement of 36 % more uniform flow than previous best study. Proposed design can fully guarantee the uniform distribution on Reynolds number range of 500–10,800, which is very robust, so it can be applied to commercial use.

Secondly, a microchannel FTS reactor model was constructed and was optimized for objectives such as reactor core volume and maximum process temperature rise. The Pareto optimal design set was obtained. It is useful and economical to set the design guideline for reactor design. An optimized reactor with a reasonable cooling-medium flowrate and the priority of fixed design parameters can also be determined. 500 LPM for C5+ 0.5 BPD was selected as the reasonable flowrate, and the order of priorities for modifying the system from the original optimal conditions was determined to be outer shell thickness > guide bar width > plate thickness. From this analysis process, more efficient industry decision making is

possible during the design of a microchannel-type reactor to be optimized for various properties.

Lastly, the superstructure model of FTS stand-alone process was constructed and optimized for maximization of profitability for sustainability. It includes the individual processes provided by previous research for maximization of carbon efficiency. The optimal design was single stage of FTS process plus partial recycle which was Section A+B. In multi-stage process, it presented basically higher carbon efficiency even for maximum profitability. However, it shows the disadvantage over whole range of reactant and product price variation against superstructure optimal. This result can provide the decision making for design of FTS process incorporated with various syngas production process.

The proposed design methodology in this thesis will be helpful to similar problem solving cases.

5.2. **Future works**

For the optimal distributor design, the number of guiding fin can be important design parameter, so that each optimal design corresponding to its variation need to be analyzed. With another point of a view, the analysis of transient study will be extended. Basically, the properties of coolant is varied in start-up and shut down procedure and even the special situation like marine condition. The flow regime can be changed in real time even though it is already guarantee the uniform distribution on steady-state.

In whole reactor design, the mechanical stress factor will be included in overall reactor optimization. It can provide more realistic result for the durability on four fixed design parameters.

In process design, the dynamic study for minimization of the duration time for start-up and shut down is required. Then, the quantitative risk assessment is also addressed for more detailed estimation of profitability.

Nomenclature

Abbreviations

ANN	artificial neural network
BPD	barrels per day
CC	cooling channel
CCH	cooling channel height (mm)
CCW	cooling channel width (mm)
CFD	computational fluid dynamics
FMZ	free mixing zone
FTS	Fischer-Trospch synthesis
GBW	guide bar width (mm)
GF	guiding fin
GSI	guide seam interval (mm)
GTL	gas to liquid
LB	lower bound
LPM	liter per minute
ME	main effect
MR	the ratio of cooling channels to process channels in manifold region
NLP	nonlinear programming
OST	outer shell thickness (mm)
PC	process channel
PCH	process channel height (mm)
PCW	process channel width (mm)
PT	plate thickness (mm)
Syngas	synthesis gas
SST	Shear stress transport
UB	upper bound
Opt	optimal

Symbol

ε	user defined constant for multi-objective optimization constraint (K)
$\Delta H_{CO\ reacted}$	CO reaction enthalpy (kJ/mole)
ΔT_{max}	process channel temperature rise based on inlet temperature (K)
ΔT_p	process channel temperature rise based on the minimum temperature in the catalytic bed (K)
ρ	fluid density (kg/m^3)
ρ_{cat}	catalyst bed density (kg/m^3)
γ_s	flow path s
γ_s^t	flow path pointer for t-th cell on flow path s
ν_{sw}	stoichiometric coefficient of component s
μ	dynamic viscosity of fluid (Pa s)
A	characteristic heat transfer area of specific adjacent cells (m^2)
b	bias vector of hidden layer
b_0	scalar bias of output layer
C_p	heat capacity of coolant (kJ/kg-K)
c(j, i, h)	coolant cell at the position of (j, i, h)
E_a	activation Energy (kJ/mol-K)
$\boldsymbol{F}^j$	surrogate model function built by ANN based on normalized j-set
F_s	molar flow rate of specific species (mol/s)
F_{avg}	average flowrate of entire channels (kg/s)
F_i	flowrate of i-th main channel [kg/s]
$F(u)$	activation function of artificial neural network
$\boldsymbol{f}_{yz}$	reactor model function based on specific ***y, z*** parameters
$[\boldsymbol{f}_s^*]j$	updated optimal Pareto optimal curve of the *j*-th set
g	gravitational acceleration (m^2/s)
h	hidden node vector
h	height (m)
k_0	kinetic constant
m_c	coolant mass flowrate of specific cell (kg/s)
n	the number of randomly selected design variable consisting of the j-th set

n	the number of cells
$n_{j,\ core}$	the number of n_j consisting of core part
N	the number of main channels
p	pressure [bar]
P	length starting from upper inlet corner along the width line of inlet manifold (mm)
P_{Div}	the number of cooling channel consisting of process channel width
P_{Num}	the number of process channels consisting of single process layer
p(j, i, h)	process cell at the position of (j, i, h)
Q	length starting from bottom inlet corner along the width line of inlet manifold (mm)
Q	heat generation of specific cell (kW)
r_w	reaction rate (mol/kg_{cat}-s)
Re	Reynolds number
s	fluid flow stream line
S	distribution index
$\mathbf{u}$	fluid velocity vector (m/s)
U	overall heat transfer coefficient of specific adjacent cells (kW/(m^2 -K))
v	flow speed (m/s)
$V_{element}$	the volume of catalyst packed cell (m^3)
$\boldsymbol{w}$	NLP optimization variable
$\mathbf{W}$	weight matrix of hidden layer
$\mathbf{W_0}$	weight vector of output layer
$\boldsymbol{x}$	design variable vector
$\boldsymbol{y}$	fixed design parameter vector
$\boldsymbol{z}$	operation parameter vector

Subscripts

α	index of fixed design parameter

c	cooling side
i	i-direction
i	index of design variable
j	j-direction
j	index of optimization set
h	h-direction
h	index of cases
opt	optimal
p	process side
s	reaction species
v	index of cases

Literature cited

1. Khalilpour, R.; Karimi, I. A., Evaluation of utilization alternatives for stranded natural gas. *Energy* **2012,** 40, (1), 317-328.

2. Park, D.; Moon, D. J.; Kim, T., Steam-CO2 reforming of methane on Ni/γ-Al2O3-deposited metallic foam catalyst for GTL-FPSO process. *Fuel Processing Technology* **2013,** 112, 28-34.

3. Lee, Y. J.; Hong, S.-I.; Moon, D. J., Studies on the steam and CO2 reforming of methane for GTL-FPSO applications. *Catalysis Today* **2011,** 174, (1), 31-36.

4. Guettel, R.; Turek, T., Comparison of different reactor types for low temperature Fischer–Tropsch synthesis: A simulation study. *Chemical Engineering Science* **2009,** 64, (5), 955-964.

5. Klemm, E.; Döring, H.; Geisselmann, A.; Schirrmeister, S., Microstructured Reactors in Heterogenous Catalysis. *Chemical Engineering & Technology* **2007,** 30, (12), 1615-1621.

6. Jarosch, K. T.; Tonkovich, A. L. Y.; Perry, S. T.; Kuhlmann, D.; Wang, Y., Microchannel Reactors for Intensifying Gas-to-Liquid Technology. In *Microreactor Technology and Process Intensification*, American Chemical Society: 2005; Vol. 914, pp 258-272.

7. Arzamendi, G.; Diéguez, P. M.; Montes, M.; Odriozola, J. A.; Falabella Sousa-Aguiar, E.; Gandía, L. M., Computational fluid dynamics study of heat transfer in a microchannel reactor for low-temperature Fischer–Tropsch synthesis. *Chemical*

Engineering Journal **2010,** 160, (3), 915-922.

8. Shin, D.-Y.; Ha, K.-S.; Park, M.-J.; Kwak, G.; Lee, Y.-J.; Jun, K.-W., CFD modeling of a modular reactor for the Fischer–Tropsch synthesis: Effectiveness of a micro-scale cross-current cooling channel. *Fuel* **2015,** 158, 826-834.

9. Shin, M.-S.; Park, N.; Park, M.-J.; Cheon, J.-Y.; Kang, J. K.; Jun, K.-W.; Ha, K.-S., Modeling a channel-type reactor with a plate heat exchanger for cobalt-based Fischer–Tropsch synthesis. *Fuel Processing Technology* **2014,** 118, 235-243.

10. Na, J.; Jung, I.; Kshetrimayum, K. S.; Park, S.; Park, C.; Han, C., Computational Fluid Dynamics Study of Channel Geometric Effect for Fischer-Tropsch Microchannel Reactor. *Korean Chemical Engineering Research* **2014,** 52, (6), 826-833.

11. Gumuslu, G.; Avci, A. K., Parametric analysis of Fischer-tropsch synthesis in a catalytic microchannel reactor. *AIChE Journal* **2012,** 58, (1), 227-235.

12. Park, S.; Jung, I.; Lee, U.; Na, J.; Kshetrimayum, K. S.; Lee, Y.; Lee, C.-J.; Han, C., Design and modeling of large-scale cross-current multichannel Fischer–Tropsch reactor using channel decomposition and cell-coupling method. *Chemical Engineering Science* **2015,** 134, 448-456.

13. Rebrov, E. V.; Schouten, J. C.; de Croon, M. H. J. M., Single-phase fluid flow distribution and heat transfer in microstructured reactors. *Chemical Engineering Science* **2011,** 66, (7), 1374-1393.

14. Tonomura, O.; Tanaka, S.; Noda, M.; Kano, M.; Hasebe, S.; Hashimoto, I., CFD-based optimal design of manifold in plate-fin microdevices. *Chemical*

Engineering Journal **2004,** 101, (1–3), 397-402.

15. Cheng, C.-H.; Huang, Y.-X.; King, S.-C.; Lee, C.-I.; Leu, C.-H., CFD (computational fluid dynamics)-based optimal design of a micro-reformer by integrating computational a fluid dynamics code using a simplified conjugate-gradient method. *Energy* **2014,** 70, 355-365.

16. Zhang, Z.; Mehendale, S.; Tian, J.; Li, Y., Experimental investigation of distributor configuration on flow maldistribution in plate-fin heat exchangers. *Applied Thermal Engineering* **2015,** 85, 111-123.

17. Pan, M.; Shao, X.; Liang, L., Analysis of Velocity Uniformity in a Single Microchannel Plate with Rectangular Manifolds at Different Entrance Velocities. *Chemical Engineering & Technology* **2013,** 36, (6), 1067-1074.

18. Pan, M.; Tang, Y.; Yu, H.; Chen, H., Modeling of velocity distribution among microchannels with triangle manifolds. *AIChE Journal* **2009,** 55, (8), 1969-1982.

19. Mohammadi, M.; Jovanovic, G. N.; Sharp, K. V., Numerical study of flow uniformity and pressure characteristics within a microchannel array with triangular manifolds. *Computers & Chemical Engineering* **2013,** 52, 134-144.

20. Wang, W.; Zhang, S.; Yang, J.; Zheng, J.; Ding, X.; Chou, M.; Tang, P.; Zhan, X., Effects of Distribution Channel Dimensions on Flow Distribution and Pressure Drop in a Plate-Fin Heat Exchanger. *Chemical Engineering & Technology* **2013,** 36, (4), 657-664.

21. Castelo Branco, D. A.; Szklo, A. S.; Schaeffer, R., Co2e emissions abatement costs of reducing natural gas flaring in Brazil by investing in offshore GTL plants

producing premium diesel. *Energy* **2010,** 35, (1), 158-167.

22. Kim, H.-J.; Choi, D.-K.; Ahn, S.-i.; Kwon, H.; Lim, H.-W.; Denholm, D.; Park, T.; Zhang, L., GTL FPSO—An Alternative Solution to Offshore Stranded Gas. **2014**.

23. Kwon, H.; Choi, D.; Moon, Y.; Ahn, S.; Jang, N.; Lim, H.; Kim, W.; Denholm, D.; Park, T., GTL FPSO & Modular GTL as Potential Solutions for Developing Offshore Oil & Gas Fields. In Offshore Technology Conference.

24. Cao, C.; Hu, J.; Li, S.; Wilcox, W.; Wang, Y., Intensified Fischer–Tropsch synthesis process with microchannel catalytic reactors. *Catalysis Today* **2009,** 140, (3–4), 149-156.

25. Dr. Volker Hessel, D. S. H., Dr. Holger Löwe, *Chemical Micro Process Engineering: Fundamentals, Modelling and Reactions*. Wiley-VCH: 2005; p 674.

26. Kolb, G.; Hessel, V., Micro-structured reactors for gas phase reactions. *Chemical Engineering Journal* **2004,** 98, (1–2), 1-38.

27. Lerou, J. J.; Tonkovich, A. L.; Silva, L.; Perry, S.; McDaniel, J., Microchannel reactor architecture enables greener processes. *Chemical Engineering Science* **2010,** 65, (1), 380-385.

28. Myrstad, R.; Eri, S.; Pfeifer, P.; Rytter, E.; Holmen, A., Fischer–Tropsch synthesis in a microstructured reactor. *Catalysis Today* **2009,** 147, Supplement, S301-S304.

29. Ostadi, M.; Dalane, K.; Rytter, E.; Hillestad, M., Conceptual design of an autonomous once-through gas-to-liquid process — Comparison between fixed bed

and microchannel reactors. *Fuel Processing Technology* **2015,** 139, 186-195.

30. Ouyang, X.; Besser, R. S., Development of a microreactor-based parallel catalyst analysis system for synthesis gas conversion. *Catalysis Today* **2003,** 84, (1–2), 33-41.

31. Chabot, G.; Guilet, R.; Cognet, P.; Gourdon, C., A mathematical modeling of catalytic milli-fixed bed reactor for Fischer–Tropsch synthesis: Influence of tube diameter on Fischer Tropsch selectivity and thermal behavior. *Chemical Engineering Science* **2015,** 127, 72-83.

32. Knochen, J.; Güttel, R.; Knobloch, C.; Turek, T., Fischer–Tropsch synthesis in milli-structured fixed-bed reactors: Experimental study and scale-up considerations. *Chemical Engineering and Processing: Process Intensification* **2010,** 49, (9), 958-964.

33. Zhu, X.; Lu, X.; Liu, X.; Hildebrandt, D.; Glasser, D., Heat transfer study with and without Fischer-Tropsch reaction in a fixed bed reactor with TiO2, SiO2, and SiC supported cobalt catalysts. *Chemical Engineering Journal* **2014,** 247, 75-84.

34. Kshetrimayum, K. S.; Jung, I.; Na, J.; Park, S.; Lee, Y.; Park, S.; Lee, C.-J.; Han, C., CFD Simulation of Microchannel Reactor Block for Fischer–Tropsch Synthesis: Effect of Coolant Type and Wall Boiling Condition on Reactor Temperature. *Industrial & Engineering Chemistry Research* **2016,** 55, (3), 543-554.

35. Shin, M.-S.; Park, N.; Park, M.-J.; Jun, K.-W.; Ha, K.-S., Computational fluid dynamics model of a modular multichannel reactor for Fischer–Tropsch synthesis: Maximum utilization of catalytic bed by microchannel heat exchangers. *Chemical*

Engineering Journal **2013,** 234, 23-32.

36. Park, S.; Jung, I.; Lee, Y.; Kshetrimayum, K. S.; Na, J.; Park, S.; Shin, S.; Ha, D.; Lee, Y.; Chung, J.; Lee, C.-J.; Han, C., Design of microchannel Fischer–Tropsch reactor using cell-coupling method: Effect of flow configurations and distribution. *Chemical Engineering Science* **2016,** 143, 63-75.

37. Deshmukh, S. R.; Tonkovich, A. L. Y.; Jarosch, K. T.; Schrader, L.; Fitzgerald, S. P.; Kilanowski, D. R.; Lerou, J. J.; Mazanec, T. J., Scale-Up of Microchannel Reactors For Fischer−Tropsch Synthesis. *Industrial & Engineering Chemistry Research* **2010,** 49, (21), 10883-10888.

38. Tonkovich, A. L. Y.; Lerou, J. J., Microstructures on Macroscale: Microchannel Reactors for Mediumand Large-Size Processes. In *Novel Concepts in Catalysis and Chemical Reactors*, Wiley-VCH Verlag GmbH & Co. KGaA: 2010; pp 239-260.

39. Rebrov, E. V.; Duinkerke, S. A.; de Croon, M. H. J. M.; Schouten, J. C., Optimization of heat transfer characteristics, flow distribution, and reaction processing for a microstructured reactor/heat-exchanger for optimal performance in platinum catalyzed ammonia oxidation. *Chemical Engineering Journal* **2003,** 93, (3), 201-216.

40. Jiao, A.; Zhang, R.; Jeong, S., Experimental investigation of header configuration on flow maldistribution in plate-fin heat exchanger. *Applied Thermal Engineering* **2003,** 23, (10), 1235-1246.

41. Jung, I.; Kshetrimayum, K. S.; Park, S.; Na, J.; Lee, Y.; An, J.; Park, S.; Lee, C.-J.; Han, C., Computational Fluid Dynamics Based Optimal Design of Guiding

Channel Geometry in U-Type Coolant Layer Manifold of Large-Scale Microchannel Fischer–Tropsch Reactor. *Industrial & Engineering Chemistry Research* **2016,** 55, (2), 505-515.

42. Wen, J.; Li, Y., Study of flow distribution and its improvement on the header of plate-fin heat exchanger. *Cryogenics* **2004,** 44, (11), 823-831.

43. Yates, I. C.; Satterfield, C. N., Intrinsic kinetics of the Fischer-Tropsch synthesis on a cobalt catalyst. *Energy & Fuels* **1991,** 5, (1), 168-173.

44. Chankong, V.; Haimes, Y. Y., Optimization-based methods for multiobjective decision-making-an overview. *Large Scale Systems In Information And Decision Technologies* **1983,** 5, (1), 1-33.

45. Steynberg, A. P.; Nel, H. G., CLEAN COAL CONVERSION OPTIONS USING FISCHER-TROPSCH TECHNOLOGY. *Fuel Chemistry Division Preprints* **2003,** 48, (1), 3.

46. Unruh, D.; Pabst, K.; Schaub, G., Fischer−Tropsch Synfuels from Biomass: Maximizing Carbon Efficiency and Hydrocarbon Yield. *Energy & Fuels* **2010,** 24, (4), 2634-2641.

47. Rafiee, A.; Panahi, M., Optimal Design of a Gas-to-Liquids Process with a Staged Fischer-Tropsch Reactor. *Chemical Engineering & Technology* **2016,** 39, (10), 1778-1784.

48. Bezemer, G. L.; Remans, T. J.; van Bavel, A. P.; Dugulan, A. I., Direct Evidence of Water-Assisted Sintering of Cobalt on Carbon Nanofiber Catalysts during Simulated Fischer−Tropsch Conditions Revealed with in Situ Mössbauer

Spectroscopy. *Journal of the American Chemical Society* **2010,** 132, (25), 8540-8541.

49. Sadeqzadeh, M.; Hong, J.; Fongarland, P.; Curulla-Ferré, D.; Luck, F.; Bousquet, J.; Schweich, D.; Khodakov, A. Y., Mechanistic Modeling of Cobalt Based Catalyst Sintering in a Fixed Bed Reactor under Different Conditions of Fischer–Tropsch Synthesis. *Industrial & Engineering Chemistry Research* **2012,** 51, (37), 11955-11964.

50. Tonkovich, A. L.; Yuschak, T.; Neagle, P. W.; Marco, J. L.; Marco, J. D.; Marchiando, M. A.; Keyes, L. W.; Deshmukh, S.; Luzenski, R. J., Laminated, Leak-Resistant Chemical Processors; Methods of Making, and Methods of Operating. In Google Patents: 2012.

51. Hargreaves, N., Smaller scale GTL The roll-out. In *World XTL Summit*, 2014.

52. Smith, R.; Loganathan, M.; Shantha, M. S., A review of the water gas shift reaction kinetics. *International Journal of Chemical Reactor Engineering* **2010,** 8, (1).

53. LeViness, S., Velocys Fischer-Tropsch Synthesis Technology – Comparison to Conventional FT Technologies. In *AIChE 2013 Spring Meeting*

13 th Topical Conference on Gas Utilization, 2013.

54. McDaniel, J., Velocys Fischer-Tropsch synthesis technology – new advances in state of the art. In *Energy Frontiers International*, 2013.

55. Seider, W. D.; Seader, J. D.; Lewin, D. R., *Product and Process Design Principles: Synthesis, Analysis and Design, 3rd Edition*. 2nd ed.; WILEY: USA,

2004.

56. Douglas, J. M., *Conceptual Design of Chemical Processes*. International ed.; McGraw-Hill: NewYork, 1988.

57. Pei, P.; Korom, S. F.; Ling, K.; Nasah, J., Cost comparison of syngas production from natural gas conversion and underground coal gasification. *Mitigation and Adaptation Strategies for Global Change* **2016,** 21, (4), 629-643.

Abstract in Korean (요 약)

천연가스를 원료로 고부가가치를 가진 액체연료로 전환하는 기술인 Gas-to-liquid(GTL) 공정은 최근 수십 년간 많은 주목을 받아왔다. 생산된 연료는 연소 후 일반적인 가솔린 또는 디젤보다 온실가스 발생량이 적으며 황함류량 또한 0.5ppm 이하로 거의 없는 수준이므로 청정연료인 동시에 친환경적인 에너지자원으로 사용될 수 있다.

GTL공정은 천연가스를 원료로 하여 일산화탄소와 수소의 혼합물인 합성가스를 제조하는 개질공정과, 이를 원료로 탄화수소체인을 합성하는 피셔트롭쉬(FTS)공정으로 나눌 수 있다. 핵심이 되는 부분이 바로 피셔트롭쉬 합성공정인데 고발열 반응(ΔH = -165 kJ/mol)이기 때문에 반응기 수준에서 효과적인 제열구조가 필수적이다. 일반적으로 상용화된 대형 GTL공정에서는 순환유동층반응기, 유동층반응기, 다관식 고정층반응기, 슬러리반응기를 이용해 조업하고 있다. 최근에는 수반가스 및 중소규모 가스전 개발용 해양플랜트를 개발하는데 있어서 해상조건에 기존반응기들이 적용되기 어렵다는 점과 중소형 규모의 공정에 대해서 경제성이 높다는 장점이 동시에 부각되어 모듈화 및 집적화도가 높은 마이크로채널 기술을 피셔트롭쉬 합성공정에 적용하는 연구가 진행되고 있다. 마이크로채널 반응기는 열 및 물질전달의 거리를 크게 줄임으로서 기존반응기

부피보다 10~ 1000배까지 줄일 수 있고, 프로세스에서 사용되는 화학물질의 효율을 높이므로 친환경적이며, 운전을 쉽게 컨트롤 할 수 있고, 전체적인 반응기 크기를 줄임으로써 공정내 집적화를 통해 공간활용도가 넓어지게 되며, 모듈화를 통하여 생산성 및 공정효율을 증가 시킬 수 있다는 장점이 있다.

본 논문에서는 마이크로채널 기술이 적용된 반응기를 최적설계하고 나아가 피셔트롭쉬 단일 공정에서 가장 경제성이 높은 구조를 도출한다. 반응기최적설계 과정에서 제열의 핵심이 되는 냉각층 분배기 최적구조를 도출하였고, 이 구조를 이용하여 반응기 코어부를 반응안전성과 소형화를 동시에 만족시킬 수 있는 최적설계안을 도출하였다. 나아가 공정적인 관점에서 마이크로채널 반응기를 도입한 초구조 공정모델링을 수행하고 최적화를 통하여 가장 경제성이 높은 반응시스템 공정안을 도출하였다. 반응기모델은 실제 반응기 운전데이터를 이용하여 타당성을 검증하였다.

먼저, 적층형 마이크로채널 반응기 내부의 냉매층에 대하여 균일한 냉매흐름을 보장하기 하기 위해 간단한 사다리꼴 형태의 가이드핀구조를 최적화하여 분배공간에 적용하였다. 가이드핀으로 유입된 냉매유체를 자유섞임공간(Free mixing zone)으로 정의된 공간으로 적절히 이송시켜 섞임을 유도는 원리를 이용하여 100개 채널이 넘는 대면적에 대해서도 안정적인 분배를 달성할 수 있었다. 구체적으로, 가이드핀의 구조에 대하여

신경망을 대리모델로 활용한 최적화를 수행하였고 나아가 최적구조에 대해서 유량, 유체종류, 운전온도에 대해서 강인성테스트를 실시한 결과 기존 연구결과 대비 $500 \leq Re\ GF \leq 10800$ 수준의 상당히 넓은 영역에서 분배의 균일성이 유지될 수 있었다.

다음으로 반응기코어부를 셀커플링(Cell-coupling) 방법을 도입하여 모델링을 수행하였고, 최대반응온도 상승폭과 반응기코어부피 최소화를 목적함수로 하여 7가지 구조변수에 대하여 다중목적최적화를 수행하였다. 최대 반응온도 상승폭은 반응기설계에서 가장 중요한 등온성(anti-hotspot)과 연관되어 있고 반응기코어부피는 반응기소형화와 직접적으로 연관되어있다. 최적화 결과로서 파레토최적점들을 얻어낼 수 있으며 반응온도 최대상승폭이 증가할수록 반응기길이는 짧아지며 너비가 증가하는 현상을 보이며 높이는 대체적으로 일정하다. 이러한 최적화 과정을 이용하여 두 가지 요소들을 결정할 수 있다. 먼저 민감도 분석을 통하여 냉매유량의 변화에 따른 파레토최적점들을 얻어 합리적인 냉매유량과 최적설계안을 동시에 도출할 수 있다. 나아가 반응기 내구성에 영향을 미치는 구조요소들의 반응기 성능에 미치는 우선순위결정을 할 수 있었다.

마지막으로 마이크로채널 반응기를 적용한 단일 피셔트롭쉬 공정을 대상으로 그간 공정효율을 높이기 위해 대표적으로 연구되었던 단일 또는 다중스테이지 피셔트롭쉬, 리사이클, 수성가스이동 반응 등의 다양한 공

정들이 적용된 초구조 공정모델을 구성하고 경제성이 높은 구조를 최적화를 통해서 도출하였다. 유전알고리즘을 사용하였으며 결론적으로 리사이클이 포함된 단일공정이 가장 경제적으로 유리한 방법임을 도출하였다. 대표적인 다른 두 시스템(다중스테이지공정, 리사이클을 포함하지 않는 단일스테이지공정)을 추가적으로 도출하여 원료비용 및 생산물가격 변화에 따른 민감도 분석을 실시한 결과, 리사이클이 포함된 단일스테이지공정이 모든 경우에 있어서 절대적으로 우위에 있음을 밝혔다.

본 연구는 마이크로채널 기술을 이용한 고발열반응기 및 피셔트롭쉬 단일공정을 설계하는데 큰 기여가 있다. 분배강인성이 높은 냉매층 최적설계 방법과 반응기의 안정적인 운전과 소형화를 동시에 만족시킬 수 있는 코어부설계 과정은 최적의 마이크로채널 반응기설계를 설계하고 운전하는데 있어서 큰 가치가 있다. 또한 경제성이 높은 피셔트롭쉬 시스템을 활용한다면 공정 전체를 설계하는 패키지로 활용될 수 있을 것이며 실제 운전시 문제점을 해결하는데 큰 도움이 될 수 있을 것이다.

주요어: 마이크로채널 반응기, 적층형 분배기, 균일분배, 반응기 최적설계, 피셔트롭쉬, 초구조 최적화, 공정설계

학번: 2014-31095

성명: 정 익 환